Solution of the Kwieciński evolution equations for unintegrated parton distributions using the Mellin transform[*]

Enrique Ruiz Arriola[†]

Departamento de Física Moderna, Universidad de Granada, E-18071 Granada, Spain

Wojciech Broniowski[‡]

The H. Niewodniczański Institute of Nuclear Physics,
Polish Academy of Sciences, PL-31342 Kraków, Poland
(Dated: March 31, 2004)

The Kwieciński equations for the QCD evolution of the unintegrated parton distributions in the transverse-coordinate space (b) are analyzed with the help of the Mellin-transform method. The equations are solved numerically in the general case, as well as in a small-b expansion which converges fast for $b\Lambda_{\rm QCD}$ sufficiently small. We also discuss the asymptotic limit of large bQ and show that the distributions generated by the evolution decrease with b according to a power law. Numerical results are presented for the pion distributions with a simple valence-like initial condition at the low scale, following from chiral large-N_c quark models. We use two models: the Spectral Quark Model and the Nambu–Jona-Lasinio model. Formal aspects of the equations, such as the analytic form of the b-dependent anomalous dimensions, their analytic structure, as well as the limits of unintegrated parton densities at $x \to 0$, $x \to 1$, and at large b, are discussed in detail. The effect of spreading of the transverse momentum with the increasing scale is confirmed, with $\langle k_\perp^2 \rangle$ growing asymptotically as $Q^2\alpha(Q^2)$. Approximate formulas for $\langle k_\perp^2 \rangle$ for each parton species is given, which may be used in practical applications.

I. INTRODUCTION

The *unintegrated* parton distributions (UPD's) have been considered in numerous works on applications of perturbative QCD [1, 2, 3, 4, 5, 6, 7, 8, 9, 10, 11, 12, 13, 14, 15, 16]. These distributions are generalizations of the usual integrated parton distributions (PD), and in some sense more basic objects, as PD's are obtained from UPD's by integration over the transverse momentum of the parton. The notion of UPD's relies on the $k_\perp$-factorization, and, in the spirit of the CCFM equations [17, 18, 19, 20], introduces two scales: the probing scale, Q, and the transverse-momentum scale, $k_\perp$. Recently, the UPD gained substantial attention, since they enter many exclusive physical processes, such as the production of the Higgs boson [21, 22], the W boson [23], heavy flavors [21, 24, 25, 26, 27], the jet production [21, 28], particle production [29], or hadron production in relativistic heavy-ion collisions [30, 31]. The unintegrated distributions were also used in studies of the longitudinal [32], charmed [33], and spin [34, 35] structure functions of the nucleon, as well as analyzed in the dipole picture of QCD [36].

The UPD's, similarly to other entities in QCD, undergo evolution with the change of the probing scale Q.

The philosophy adopted here is similar to the case of the integrated PD. At some initial scale Q_0 we need to know the non-perturbative quantity from measurements, models, or lattice calculations, and then we can evolve it to a different scale Q with the help of suitable QCD evolution equations. In the case of integrated PD we need to assume the dependence of PD on the Bjorken x variable at the initial scale Q_0. For the UPD we need to know in addition the dependence on the transverse momentum, $k_\perp$, or, equivalently, the transverse coordinate b, which is the variable Fourier-conjugated to $k_\perp$. Knowing this, we compute, with no extra physical input apart for the assumptions entering the QCD evolution, the unintegrated distribution at the final scale Q.

Important physics questions may be answered. In particular, the UPD evolve in such a way that the average transverse-momentum increases in a specified way with the scale [14, 15, 16, 21]. This spreading can be studied quantitatively within the approach. This constrains the freedom in phenomenological analyses of processes involving the UPD's.

In his studies of the problem, Kwieciński started from the CCFM formalism [17, 18, 19, 20], which explicitly involves two separate scales: the probing scale, Q, and the transverse momentum of the parton, $k_\perp$. The CCFM equations were subsequently extended to include the quarks, as well as reduced to the single-loop approximation. In addition, the non-Sudakov form factor was dropped. Kwieciński found that in this approximation the equations diagonalize in the space Fourier-conjugated to the transverse momentum, where they assume a par-

ticularly simple and elegant form in a close resemblance of the DGLAP [37, 38, 39, 40] equations for the integrated PD. The only, but most important, difference is the appearance of the Bessel function $J_0(Qb)$ in the evolution kernel. Thus, the evolution depends on the transverse coordinate b. In the original work of Ref. [16] these equations were called "the CCFM equations for the UPD in the transverse-coordinate space in the single-loop approximation". Due to numerous steps leading away from the original CCFM, we find it more appropriate to call the equations of Refs. [16] *the Kwieciński equations for the UPD evolution.* Since in the case of integrated PD these equations reduce to the usual LO DGLAP, the range of applicability of the Kwieciński equations is not larger as for the LO DGLAP, with not too small and not too large values of the Bjorken x variable.

Formally, the Kwieciński equations are integro-differential equations with the kernel depending on the transverse coordinate b (*cf.* Sec. II). As such, they are not trivial to solve numerically. The method of the original works [14, 15, 16] involved the Chebyshev interpolation in the x and Q spaces for each value of b. In this paper we offer an alternative method, based on the evolution of the x-moments of UPD. In the moment (Mellin) space, the evolution equations become a set of ordinary differential equations, which can be solved numerically in a very efficient way (see Sec. III). We derive analytic expressions for the b-dependent anomalous dimensions, which can be written in terms of hypergeometric functions. Then, the inverse Mellin transform to the original x-space is performed via numerical integration with oscillatory functions. We show that the procedure is fast and stable, providing a useful numerical tool for evolving the UPD.

The Mellin-transform method allows us to carry analytic considerations, such as studies of certain limits of the equations, specifically the cases of low and and large b, and x approaching the endpoints. We pursue these considerations, which can be done since the form of the b-dependent anomalous dimensions is analytic.

In addition to developing a different numerical method (Sec. III), our study differs from Ref. [16] in two physical aspects. Firstly, rather than guessing the initial shape in b, we use the results of low-energy chiral quark models (Sec. IV). We consider two models: the recently proposed Spectral Quark Model of Ref. [41, 42, 43] and the Nambu–Jona-Lasinio model with the Pauli Villars regularization [44]. These models were used before to describe the integrated PD [45, 46, 47, 48], and were shown to do a surprisingly good job, in particular for the valence distribution in the pion. They were also used to describe successfully other aspect of high-energy processes, such as the pion distribution amplitude [49] and generalized (off-forward) PD of the pion [50, 51]. The models give the initial condition at the model scale Q_0 in a particularly simple, factorized form. The valence quarks are distributed uniformly in x, while the gluons and the sea quarks vanish. The b-dependence is a simple, analytic

function with exponential fall-off at large b. We stress that the b dependence is a prediction of the model, rather than a mere guess, as is frequently made. Secondly, our implementation of the evolution switches from three to four flavors above the charm-production threshold, customarily taken at $Q^2 = 4$ GeV^2. Our numerical results are presented in Sec. V, where we show the dependence of the UPD's on x and b.

Since the analytic forms of the anomalous dimensions involve generalized hypergeometric functions, which may be cumbersome to program, we have developed a low-b expansion (Sec. VI), which makes the calculations simpler when b is not too large. The expansion is in powers of $b\Lambda_{\mathrm{QCD}}$, and is fast and stable. For the opposite problem, where Qb is large, we have obtained asymptotic expansions (Sec. VII), which allow to deal numerically with the generalized hypergeometric functions.

Our method of solving the equations in the Mellin space carries additional bonuses. In particular, it allows us for analytic considerations in the investigation of formal limits at $x \to 1$ (Sec. VIII) and $x \to 0$ (Sec. IX). At $x \to 1$ we show that the b-dependent non-singlet distribution approaches very fast the integrated non-singlet distrtibution. At $x \to 0$ we find generalizations of the double-leading-logarithm (DLLA) formulas of Ref. [54]. Finally, we examine the large-b behavior, where we show that the evolution-generated UPD's from the Kwieciński equations exhibit power-law behavior at large b. The fall-off is much faster for the gluons than for the quarks.

Widening in the transverse momentum of all partonic distributions is confirmed. We show that $\langle k_\perp^2 \rangle$ grows with the probing scale as $Q^2 \alpha(Q^2)$. We write an approximating formula for the width for each partonic species, which may be useful in practical applications with the pion (Sec. X). The widening effect becomes stronger and stronger as Q increases or x decreases, and it is bigger for the gluons than for the non-singlet and singlet quarks (see Sec. X).

The numerical method of this paper, which is easy to program and numerically fast and efficient, can be used for other initial conditions as well, for instance for the GRS [52] parameterization of the pion or the GRV parameterization [53], of the nucleon, supplied with a profile in the transverse coordinate, as originally studied in Ref. [16]. The only difference is in the form of the initial Mellin moments, which acquire the dependence on b. General prediction of the method in formal limits are listed in Sec. XI.

Appendices contain many technical details, such as the perturbative QCD parameters and splitting functions (App. A), the analytic form of the b-dependent anomalous dimensions which enter the evolution in the Mellin space (App. B), their low-b (App. C) and high-b expansion (App. D), as well as the pole-residue expansion (App. E). The latter is useful in analytic considerations near $x = 0$.

II.   THE KWIECIŃSKI EQUATIONS

In his studies of the UPD's, Kwieciński [14, 15, 16, 22] started from the CCFM formalism [17, 18, 19, 20] explicitly involving two separate scales: the probing scale, Q, and the transverse momentum of the parton, $k_\perp$. Then, the original CCFM equations were supplemented with the quarks, as well as reduced to the single-loop approximation. The latter approximation replaces the angular ordering of the emitted gluons with the ordering of their transverse momenta. In addition, the non-Sudakov form factor was dropped. Kwieciński realized that the evolution equations for the UPD's acquire a particularly simple form in the transverse-coordinate space, b, conjugated to the transverse momentum $k_\perp$. For each distribution one introduces

$$f_j(x,b,Q) = \int_0^\infty 2\pi dk_\perp\, k_\perp\, J_0(bk_\perp)\, f_j(x,k_\perp,Q), \quad (2.1)$$

where $j = NS$ (non-singlet quarks), S (singlet quarks), or G (gluons), and J_0 is the Bessel function. In order to avoid confusion, we stress that the transverse coordinate b, conjugated to the parton's transverse momentum, is not the impact parameter, appearing in the analysis of the generalized PD. The latter quantity is conjugated the the transverse momentum transfer in off-forward scattering processes.

At $b = 0$ the functions f_j are related to the integrated parton distributions, $p_j(x,Q)$, as follows:

$$f_j(x,0,Q) = \frac{x}{2}p_j(x,Q). \quad (2.2)$$

More explicitly, for the case of the pion studied in this paper (we take π^+ for definiteness) we have

$$\begin{aligned}
p_{\mathrm{NS}} &= \bar{u} - u + d - \bar{d}, \\
p_S &= \bar{u} + u + d + \bar{d} + \bar{s} + s + ..., \\
p_{\mathrm{sea}} &\equiv p_S - p_{\mathrm{NS}} = 2\bar{d} + 2u + \bar{s} + s + ..., \\
p_G &= g,
\end{aligned} \quad (2.3)$$

where ... stand for higher flavors.

The Kwieciński equations read [16]:

$$\begin{aligned}
Q^2\frac{\partial f_{\mathrm{NS}}(x,b,Q)}{\partial Q^2} &= \frac{\alpha_s(Q^2)}{2\pi}\int_0^1 dz\, P_{qq}(z)\left[\Theta(z-x)\,J_0((1-z)Qb)\,f_{\mathrm{NS}}\left(\frac{x}{z},b,Q\right) - f_{\mathrm{NS}}(x,b,Q)\right] \\
Q^2\frac{\partial f_S(x,b,Q)}{\partial Q^2} &= \frac{\alpha_s(Q^2)}{2\pi}\int_0^1 dz\left\{\Theta(z-x)\,J_0((1-z)Qb)\left[P_{qq}(z)\,f_S\left(\frac{x}{z},b,Q\right) + P_{qG}(z)\,f_G\left(\frac{x}{z},b,Q\right)\right]\right. \\
&\quad \left. - [zP_{qq}(z) + zP_{Gq}(z)]\,f_S(x,b,Q)\right\} \\
Q^2\frac{\partial f_G(x,b,Q)}{\partial Q^2} &= \frac{\alpha_s(Q^2)}{2\pi}\int_0^1 dz\left\{\Theta(z-x)\,J_0((1-z)Qb)\left[P_{Gq}(z)\,f_S\left(\frac{x}{z},b,Q\right) + P_{GG}(z)\,f_G\left(\frac{x}{z},b,Q\right)\right]\right. \\
&\quad \left. - [zP_{GG}(z) + zP_{qG}(z)]\,f_G(x,b,Q)\right\}
\end{aligned} \quad (2.4)$$

The splitting functions $P_{ab}(z)$ are listed in Eq. (A9).

Following Ref. [16], a factorized form of the distribution functions at the initial scale Q_0 is assumed,

$$f_j(x,b,Q_0) = F^{\mathrm{NP}}(b)\frac{x}{2}p_j(x,Q_0), \quad (2.5)$$

with the profile function $F^{\mathrm{NP}}(b)$ taken to be universal for all species of partons. The factorization assumption (2.5) is technical and one can easily depart from this limitation in numerical studies. We note, however, that the models of Ref. [42, 44], studied in Sec. IV, do predict a factorized initial condition of the form (2.5). The input profile function, $F^{\mathrm{NP}}(b)$, is linked through the Fourier-Bessel transform to the $k_\perp$ distribution at the scale Q_0. At $b = 0$ the normalization is $F^{\mathrm{NP}}(0) = 1$. The profile function factorizes from the evolution equations. This is clear, since any solution of Eq. (2.4) remains a solution when multiplied by an arbitrary function of b. Due to evolution, at higher scales Q we have

$$f_j(x,b,Q) = F^{\mathrm{NP}}(b)f_j^{\mathrm{evol}}(x,b,Q), \quad (2.6)$$

with $f_j^{\mathrm{evol}}(x,b,Q)$ satisfying equations *identical* to (2.4).

We should stress again an important physical difference between $F^{\mathrm{NP}}(b)$ and $f_j^{\mathrm{evol}}(x,b,Q)$. While $F^{\mathrm{NP}}(b)$ originates entirely from low-energy, *non-perturbative* physics, $f_j^{\mathrm{evol}}(x,b,Q)$ is given by the *perturbative QCD evolution* with Eq. (2.4) from the initial condition

$$f_j^{\mathrm{evol}}(x,b,Q_0) = \frac{x}{2}p_j(x,Q_0). \quad (2.7)$$

Throughout this paper, except for Sec. IV, we focus on the perturbative evolution and the functions $f_j^{\mathrm{evol}}(x,b,Q)$. The function $F^{\mathrm{NP}}(b)$ is referred to as *the*

4

initial profile and $f_j^{\text{evol}}(x, b, Q)$ as *the evolution-generated UPD*.

III.   THE KWIECIŃSKI EQUATION IN THE MELLIN SPACE

We define the x-moments of an unintegrated parton distribution in the impact parameter space as (we retain the same symbol for the function and its Mellin transform, hoping the distinction made by the argument prevents any confusion)

$$f_j(n, b, Q) = \int_0^1 dx\, x^{n-1} f_j(x, b, Q). \qquad (3.1)$$

In the Mellin space, the evolution equations for the UPD are very simple, as they become diagonal both in b and n. They involve b-dependent anomalous dimensions, equal to

$$\gamma_{n,ab}(Qb) = 4\int_0^1 dz\, [z^n J_0\left((1-z)Qb\right) - 1] P_{ab}(z)$$
$$= \gamma_{n,ab}^{(0)} - 4\int_0^1 dz\, z^n [J_0\left((1-z)Qb\right) - 1] P_{ab}(z),$$
$$(3.2)$$

where the values at $b = 0$ are

$$\gamma_{n,NS}^{(0)} = -4\int_0^1 dz(z^n - 1)P_{qq}(z),$$
$$\gamma_{n,qq}^{(0)} = -4\int_0^1 dz\, [(z^n - z)P_{qq} - zP_{Gq}],$$
$$\gamma_{n,qG}^{(0)} = -4\int_0^1 dz z^n P_{qG}, \qquad (3.3)$$
$$\gamma_{n,Gq}^{(0)} = -4\int_0^1 dz z^n P_{Gq},$$
$$\gamma_{n,GG}^{(0)} = -4\int_0^1 dz\, [(z^n - z)P_{GG} - zP_{qG}].$$

Their explicit form for various channels is listed in Eq. (B6,B7). The fact that we can write the analytic form of the integrals in Eq. (3.2) (see App. B) allows for efficient numerical calculations and analytic considerations.

The integration of both sides of Eq. (2.4) with $\int_0^1 dx x^{n-1}$ yields for the non-singlet case the equation

$$\frac{df_{\text{NS}}(n, b, Q)}{dQ^2} = -\frac{\alpha_S(Q^2)}{8\pi Q^2}\gamma_{n,NS}(Qb)f_{\text{NS}}(n, b, Q). \quad (3.4)$$

The formal solution of Eq. (3.4) can be readily obtained as

$$\frac{f_{\text{NS}}(n, b, Q)}{f_{\text{NS}}(n, b, Q_0)} = \exp\left[-\int_{Q_0^2}^{Q^2} \frac{dQ'^2 \alpha(Q'^2)}{8\pi Q'^2}\gamma_{\text{NS}}(n, b, Q')\right]. \quad (3.5)$$

In the singlet channel we find the coupled set of equations,

$$\frac{df_S(n, b, Q)}{dQ^2} = -\frac{\alpha_S(Q^2)}{8\pi Q^2}$$
$$\times [\gamma_{n,qq}(Qb)f_S(n, b, Q) + \gamma_{n,qG}(Qb)f_G(n, b, Q)],$$
$$\frac{df_G(n, b, Q)}{dQ^2} = -\frac{\alpha_S(Q^2)}{8\pi Q^2}$$
$$\times [\gamma_{n,Gq}(Qb)f_S(n, b, Q) + \gamma_{n,GG}(Qb)f_G(n, b, Q)],$$
$$(3.6)$$

which has the formal solution

$$\begin{pmatrix} f_S(n, b, Q) \\ f_G(n, b, Q) \end{pmatrix} = \qquad (3.7)$$
$$\mathcal{P}\exp\left[-\int_{Q_0^2}^{Q^2} \frac{dQ'^2\alpha(Q'^2)}{8\pi Q'^2}\Gamma_n(Qb)\right]\begin{pmatrix} f_S(n, b, Q_0) \\ f_G(n, b, Q_0) \end{pmatrix},$$
$$\Gamma_n(Qb) = \begin{pmatrix} \gamma_{n,qq}(Qb) & \gamma_{n,qG}(Qb) \\ \gamma_{n,Gq}(Qb) & \gamma_{n,GG}(Qb) \end{pmatrix}.$$

The symbol $\mathcal{P}$ indicates that powers of Γ_n are ordered along the integration path. The qualitative difference between Eq. (3.7) and the LO DGLAP equations is the fact that Γ_n depends on the evolution variable Q. This makes the singlet sector more difficult to analyze analytically. Equations (3.6) can be solved numerically for any value of n real or complex [55]. For the case of integrated PD ($b = 0$) Eq. (3.4) and (3.6) reduce to the well-known LO DGLAP equation in the Mellin space.

The corresponding UPD in the x space can be reconstructed using the inverse Mellin transform,

$$f_j(x, b, Q) = \int_{n_0-i\infty}^{n_0+i\infty} \frac{dn}{2\pi i}x^{-n} f_j(n, b, Q), \qquad (3.8)$$

where n_0 has to be chosen in such a way as to leave all the singularities on the left-hand-side of the contour. It turns out that for $b \neq 0$ the analytic structure of the $b-$dependent anomalous dimension remains the same as for the $b = 0$ case. This can be inferred directly by studying the analytic structure of the formulas (B6,B7) or the pole-residue expansion of Eq. (E4). Thus, we have the result that that $\gamma_{n,NS}(Qb)$, $\gamma_{n,qq}(Qb)$, and $\gamma_{n,qG}(Qb)$ have poles at $n = -1, -2, -3, ...$, while $\gamma_{n,GG}(Qb)$ and $\gamma_{n,Gq}(Qb)$ have poles at $n = 0, -1, -2, ...$ Parameterizing the contour in Eq. (3.8) as $n = n_0 + it$, we arrive at the inversion formula

$$f_j(x, b, Q) = x^{-n_0}\int_0^\infty \frac{dt}{\pi}\left(\cos(t\log x)\text{Re}[f_j(n_0 + it, b, Q)]\right.$$
$$\left. + \sin(t\log x)\text{Im}[f_j(n_0 + it, b, Q)]\right). \qquad (3.9)$$

For the non-singlet case we take $n_0 = 0$, while for the singlet case $n_0 = 1$. As an additional check we have also verified that a bended integration path $n = c + re^{i\pi/4}$ with $0 \leq r < \infty$, as used in [55], also works nicely.

IV. THE INITIAL CONDITION FOR THE UPD OF THE PION

As an illustration of our method, we consider the UPD's of the pion with the initial condition at Q_0 provided by two large-N_c low-energy chiral quark models. The original work of Ref. [16] tested the GRS parameterization for the pion [52] and the GRV parameterization for the nucleon [53], supplied with a Gaussian profile $F^{\rm NP}(b)$. The considered models generate the functions $F^{\rm NP}(b)$ as genuine model predictions of low-energy non-perturbative physics, with no freedom involved. Our first model is the recently proposed Spectral Quark Model (SQM)[41, 42, 43], and the second one is the popular Nambu–Jona Lasinio model (NJL) with the Pauli-Villars regularization [44], treated for simplicity in the strict chiral limit.

Firstly, since the chiral quark models have no gluon degrees of freedom, we have at the model scale

$$g(x, Q_0) = 0, \qquad (4.1)$$

or

$$f_G^{\rm evol}(x, b, Q_0) = 0. \qquad (4.2)$$

For the integrated valence quark PD both models predict, in the chiral limit and at the model scale Q_0, that

$$q(x, Q_0) = \theta(x)\theta(1 - x), \qquad (4.3)$$

i.e. a constant value with the proper normalization and support. Thus the corresponding $f^{\rm evol}$ functions of Eq. (2.2) are linear in x,

$$f_{NS,S}^{\rm evol}(x, b, Q_0) = x\theta(x)\theta(1 - x), \qquad (4.4)$$

The scale of the model, as found from the momentum sum-rule, is rather low: $Q_0 = 313$ MeV. Although this is admittedly a very low scale, one may hope that the typical expansion parameter, $\alpha(Q_0^2)/(2\pi) \sim 0.3$, is low enough to make the perturbation theory sensible. This claim gains support from the next-too-leading analysis of the integrated PD [45], where the corrections are found to be small.

The QCD evolution is crucial for the phenomenological success of the considered low-energy chiral quark models. In Refs. [45, 46, 47] it has been found that the non-singlet distribution, when evolved to the scale of 2 GeV, agrees very well with the SMRS parameterization of the pion data [56], while in [57] it has been very favorably compared to the old E615 data at 4 GeV [58] (see the discussion in Sec. V and Fig. 5).

In the SQM, the valence UPD of the pion at the scale Q_0 is [42]

$$
\begin{aligned}
q(x, k_\perp, Q_0) &= \overline{q}(1 - x, k_\perp) \qquad (4.5) \\
&= \frac{6M_V^3}{\pi(k_\perp^2 + M_V^2/4)^{5/2}}\theta(x)\theta(1 - x),
\end{aligned}
$$

where $M_V = 770$ MeV is the mass of the ρ meson. Passing to the impact-parameter space with the Fourier-Bessel transform yields

$$
\begin{aligned}
q(x, b, Q_0) &\equiv 2\pi \int_0^\infty k_\perp dk_\perp q(x, k_\perp) J_0(k_\perp b) \qquad (4.6) \\
&= \left(1 + \frac{bM_V}{2}\right)\exp\left(-\frac{M_V b}{2}\right)\theta(x)\theta(1 - x).
\end{aligned}
$$

The expansion at small b gives

$$
\begin{aligned}
q(x, b, Q_0) &= \left(1 - \frac{M_V^2 b^2}{8} + \frac{M_V^3 b^3}{24} + \dots\right) \\
&\quad \times \theta(x)\theta(1 - x), \qquad (4.7)
\end{aligned}
$$

and average transverse momentum squared is equal to

$$
\begin{aligned}
\langle k_\perp^2 \rangle_{\rm NP}^{\rm SQM} &\equiv \frac{\int d^2 k_\perp\, k_\perp^2\, q(x, k_\perp)}{\int d^2 k_\perp\, q(x, k_\perp)} = -\frac{4}{q(x, b)}\left.\frac{dq(x, b)}{db^2}\right|_{b=0} \\
&= \frac{M_V^2}{2}, \qquad (4.8)
\end{aligned}
$$

which numerically gives $\langle k_\perp^2 \rangle_{\rm NP}^{\rm SQM} = (544\text{ MeV})^2$ (all at the model working scale Q_0). The subscript *NP* reminds us that the quantity comes entirely from the non-perturbative physics, entering profile function $F^{\rm NP}(b)$ (see the discussion at the end of Sec. II).

In the NJL model with the PV regularization [44] the analogous formulas read [48]

$$
\begin{aligned}
q(x, k_\perp, Q_0) &= \overline{q}(1 - x, k_\perp) \qquad (4.9) \\
&= \frac{\Lambda^4 M^2 N_c}{4f_\pi^2 \pi^3 (k_\perp^2 + M^2)(k_\perp^2 + \Lambda^2 + M^2)^2}\theta(x)\theta(1 - x),
\end{aligned}
$$

$$
\begin{aligned}
q(x, b, Q_0) &= \frac{M^2 N_c}{4f_\pi^2 \pi^2}\left(2K_0(bM) - 2K_0(b\sqrt{\Lambda^2 + M^2})\right. \\
&\quad \left. - \frac{b\Lambda^2 K_1(b\sqrt{\Lambda^2 + M^2})}{\sqrt{\Lambda^2 + M^2}}\right)\theta(x)\theta(1 - x),
\end{aligned}
$$
$$(4.10)$$

where the pion decay constant is given by

$$f_\pi^2 = \frac{M^2 N_c\left(\Lambda^2 + \left(\Lambda^2 + M^2\right)\log\frac{\Lambda^2 + M^2}{M^2}\right)}{4\pi^2\left(\Lambda^2 + M^2\right)}. \qquad (4.11)$$

The parameters of the model are adjusted in such a way that $f_\pi = 93$ MeV, namely $M = 280$ MeV and $\Lambda = 871$ MeV. The expansion at small b yields

$$q(x, b, Q_0) = \qquad (4.12)$$
$$\left(1 - \frac{M^2 N_c\left(\Lambda^2 - M^2\log\frac{\Lambda^2 + M^2}{M^2}\right)b^2}{16\pi^2 f_\pi^2} + \dots\right)$$
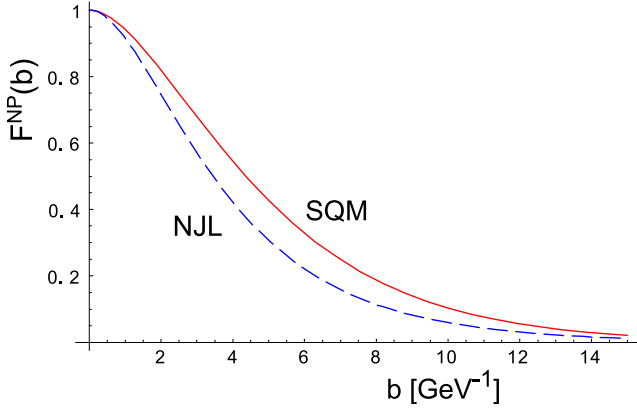$$\times \theta(x)\theta(1 - x),$$

FIG. 1: The initial profile functions F_{NP} for the SQM and NJL models, plotted as functions of the transverse coordinate b. The fall-off is exponential, according to Eq. (4.14) and (4.10).

and average transverse momentum squared is equal to

$$\langle k_\perp^2 \rangle_{\mathrm{NP}}^{\mathrm{NJL}} = \frac{M^2 N_c \left(\Lambda^2 - M^2 \log \frac{\Lambda^2 + M^2}{M^2} \right)}{4\pi^2 f_\pi^2}, \quad (4.13)$$

which numerically gives $\langle k_\perp^2 \rangle_{\mathrm{NP}}^{NJL} = (626 \text{ MeV})^2$ (at the scale Q_0), which is similar to the number from the SQM.

Finally, in the notation of Eq. (2.6) we can write that the initial profile function is

$$F_{\mathrm{SQM}}^{\mathrm{NP}}(b) = \left(1 + \frac{bM_V}{2} \right) \exp\left(-\frac{M_V b}{2} \right), \quad (4.14)$$

$$F_{\mathrm{NJL}}^{\mathrm{NP}}(b) = \frac{M^2 N_c}{4 f_\pi^2 \pi^2} \left(2K_0(bM) - 2K_0(b\sqrt{\Lambda^2 + M^2}) \right.$$
$$\left. - \frac{b\Lambda^2 K_1(b\sqrt{\Lambda^2 + M^2})}{\sqrt{\Lambda^2 + M^2}} \right). \quad (4.15)$$

Both initial profile functions are displayed in Fig. 1. Note that the profiles, although have a b^2 correction at small b, are not Gaussian, and at large b display an exponential fall-off.

As discussed in Sec. II, the form of $F^{\mathrm{NP}}(b)$ factorizes from the evolution. In both models there is no dependence of UPD on x at the initial scale Q_0. As a results, we get the following set of initial moments:

$$f_{\mathrm{NS}}^{\mathrm{evol}}(n, b, Q_0) = \frac{1}{n+1},$$
$$f_{S}^{\mathrm{evol}}(n, b, Q_0) = \frac{1}{n+1},$$
$$f_{G}^{\mathrm{evol}}(n, b, Q_0) = 0. \quad (4.16)$$

We remark that away from the chiral limit the separability of the dependence on x and b no longer holds. In this case the initial conditions for the evolution are more complicated (they depend on b), but the analysis can be easily generalized to account for this case as well.
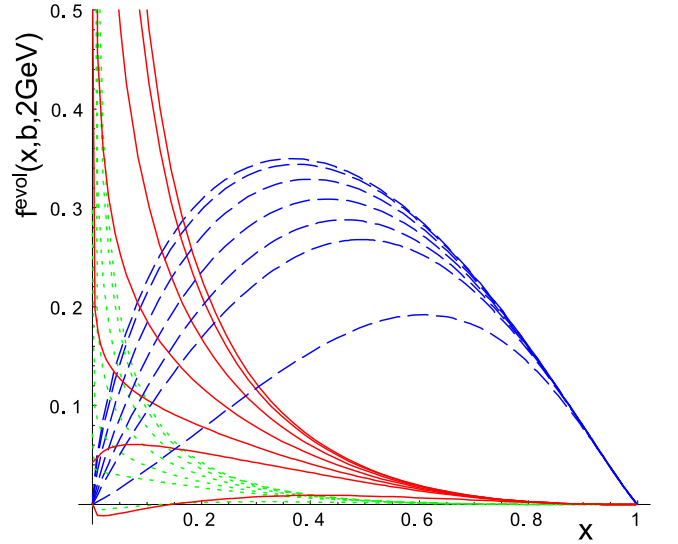

FIG. 2: The evolution-generated UPD's for the pion for various values of the transverse coordinate (from top to bottom $b = 0, 1, 2, 3, 4, 5$ and 10 GeV^{-1}), plotted as functions of the Bjorken x. The evolution is made with the initial condition (4.4) at $Q_0 = 313$ MeV up to $Q = 2$ GeV. Solid lines – gluons, dashed lines – valence quarks, dotted lines – sea quarks.

V. NUMERICAL RESULTS

In Fig. 2 we present the results of our numerical calculation with the method using the Mellin transform. The initial conditions are for the pion in the chiral limit (4.16), holding at $Q_0 = 313$ MeV, and the evolution is carried up to the scale of $Q = 2$ GeV. The differential equations for the moments, (3.4,3.6), are solved numerically for complex n−values along the Mellin contour, and subsequently the inverse Mellin transform (3.9) is carried out. The figure contains three families of curves, solid for the gluon, dashed for the valence quarks, and dotted for the sea quarks. In each family b assumes the values 0, 1, 2, 3, 4, 5, and 10. Naturally, increasing b results in a decrease of the distribution, with the effect strongest at low x. At x close to 1 this effect disappears, which is explained in Sec. VIII. We also note that at high values of b the distributions for the gluons become negative, reflecting the change of sign of the Bessel function in the evolution kernel of Eq. (2.4). As already discussed in Ref. [16], this poses no immediate physical problems, as the distributions in $k_\perp$ remain positive as primary objects, and so are the physical cross sections.

The results of Fig. 2 are consistent with the findings of Ref. [16], where a different numerical method was used, as well as a different initial condition tested.

In Fig. 3 we show the dependence of the evolution-generated UPD's on b at $Q = 2$ GeV and $x = 0.1$. The results are represented by squares for the non-singlet quarks, diamonds for the singlet quarks, and stars for the gluons. We note the much faster fall-off with b for the gluons than for the quarks, as expected from Eq. (7.8). The
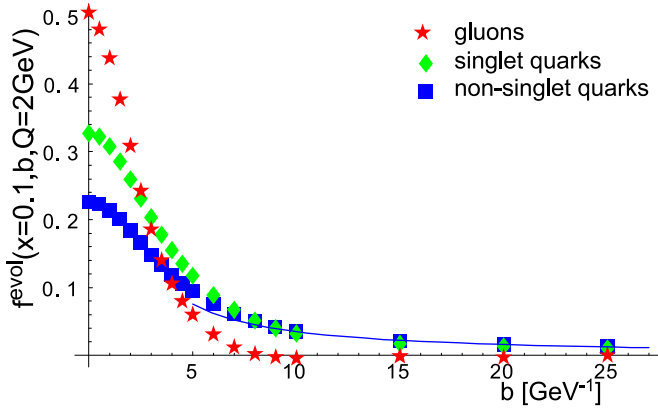
FIG. 3: Evolution-generated UPD's for the pion for $Q = 2$ GeV and $x = 0.1$, plotted as functions of b. The evolution is made with the initial condition (4.4) at $Q_0 = 313$ MeV. The numerical results are represented by squares for the non-singlet quarks, diamond for the singlet quarks, and stars for the gluons, while the solid line shows the asymptotic formula (7.5 for the case of non-singlet quarks. We note the much faster fall-of for the gluons than for the quarks, as expected from Eq. (7.8). The quarks exhibit a long-range tail, according to the power-law formula (7.5). As Q is increased or x decreased, the distributions in b become narrower, leading to spreading in $k_\perp$.
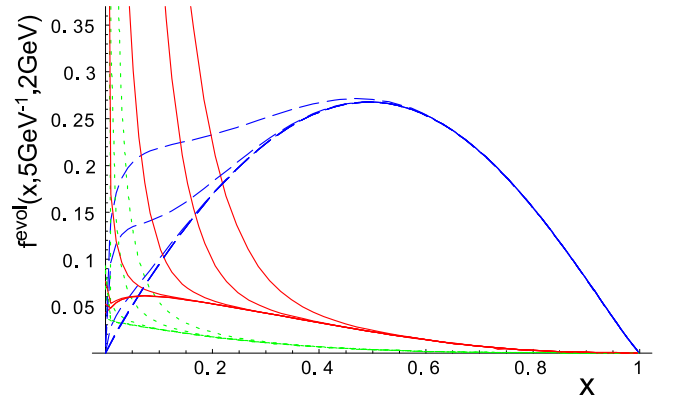

FIG. 4: The low-b expansion for the evolution-generated UPD's of the pion at $b = 5$ GeV^{-1} and $Q = 2$ GeV^2, plotted as a function of the Bjorken x. Solid lines – gluons, dashed lines – valence quarks, dotted lines – sea quarks. For each kind of parton the curves from top to bottom correspond to 2, 4, 6, 8, 10, and 16 terms in the small b-expansion. The initial condition for the evolution is provided by Eq. (4.4).

quarks exhibit a long-range tail, according to the power-law formula (7.5). The solid line shows the asymptotic form for the case of non-singlet quarks from Eq. (7.5,7.6) (see Sec. VII), which becomes accurate for $b \geq 10$ GeV^{-1}. As Q is increased further, or x decreased, the distributions in b become narrower, leading to larger spreading in $k_\perp$. For more details and plots concerning other numerical results see Ref. [16].

VI. LOW-b EXPANSION

Since the anomalous dimensions (B6,B7) involve generalized hypergeometric functions, they are not easy to use in numerical calculations. For that reason we consider the small-b expansion, as well as the asymptotic forms at large bQ, presented in the next section. It is convenient to introduce the notation

$$ r_k = r_k(Q_0^2, Q^2) = \int_{Q_0^2}^{Q^2} \frac{dQ'^2 \alpha(Q'^2)}{8\pi Q'^2} Q'^{2k}. $$
(6.1)

The explicit form of functions r_k is given in Appendix A. Next, we apply Eq. (C5) and find the following expansion in the non-singlet channel:

$$ \frac{f(n,b,Q)}{f(n,b,Q_0)} = e^{\gamma_{n,NS}^{(0)} r_0} \exp\left[-C_F \sum_{k=1}^{\infty} \frac{(-b^2)^k 4^{1-k}}{k!^2} \right. $$
$$ \left. \times \left[B(2k,n+1) + B(2k,n+3) \right] r_k \right], $$
(6.2)

where B is the Euler beta function. We note that although at the level of the differential equation our expansion is formally in Qb, the result (6.2), together with the fact that r_k is proportional to Λ_{QCD}^{2k} (cf. (A4)), show that the expansion parameter is actually $b\Lambda_{QCD}$. The rate of convergence of the method can be deduced from Fig. (4). As we can see, the number of terms needed increases for increasing b and decreasing x. For $x > 0.01$ eight terms in the expansion seems more than sufficient.

VII. LARGE-b EXPANSION

Appendix D contains asymptotic forms of the generalized hypergeometric functions and of the b-dependent anomalous dimensions. These expressions hold in the limit of large Qb at n kept fixed. The formulas are of great practical importance in the present study, since they are much simpler to implement in numerical calculations than the generalized hypergeometric functions appearing in Eq. (B6,B7). Actually, Eq. (D3-D6) should be used whenever Qb is larger than about $10|n|$. Since in practical problems the scale Q may be as large as the mass of the W-boson, there is a frequent need to use the asymptotic expressions (D3-D6). Also, if the UPD's in the transverse momentum are needed, one has to carry back the Fourier transform from the b-space to the $k_\perp$-space, which involves all values of b.

We start with the non-singlet case of Eq. (3.4). With the help of Eq. (D3), where at the leading order in $1/(Qb)$ we drop the oscillatory parts, we may write (3.5) at large Qb:

$$ \frac{f_{NS}^{evol}(n,b,Q)}{f_{NS}^{evol}(n,b,Q_0)} = e^{y_0 + y_1 n}, $$
(7.1)

where

$$y_1 = -4C_F \left(\frac{2\Lambda_{\text{QCD}}^2}{b} - \frac{1}{b^3} \right) r_{-3/2}(Q_0^2, Q^2),$$

$$y_0 = -4C_F \left(\frac{2\Lambda_{\text{QCD}}^2}{b} r_{-3/2}(Q_0^2, Q^2) + \frac{1}{\beta_0^{(3)}} \log \frac{Q}{Q_0} \right.$$
$$\left. + 2 \left[\log \frac{b\Lambda_{\text{QCD}}}{2} + \gamma - \frac{3}{4} \right] r_0(Q_0^2, Q^2) \right),$$
$$\text{for } Q^2 < \mu_c^2, \quad (7.2)$$

and

$$y_1 = -4C_F \left(\frac{2\Lambda_{\text{QCD}}^2}{b} r_{-3/2}(Q_0^2, \mu_c^2) \right.$$
$$\left. + \frac{2\Lambda_4^2}{b} r_{-3/2}(\mu_c^2, Q^2) - \frac{1}{b^3} r_{-3/2}(Q_0^2, Q^2) \right),$$

$$y_0 = -4C_F \left(\frac{2\Lambda_{\text{QCD}}^2}{b} r_{-3/2}(Q_0^2, \mu_c^2) \right.$$
$$+ \frac{2\Lambda_4^2}{b} r_{-3/2}(\mu_c^2, Q^2) + \frac{1}{\beta_0^{(3)}} \log \frac{\mu_c}{Q_0} + \frac{1}{\beta_0^{(4)}} \log \frac{Q}{\mu_c}$$
$$+ 2 \left[\log \frac{b\Lambda_{\text{QCD}}}{2} \right] r_0(Q_0^2, \mu_c^2)$$
$$\left. + 2 \left[\log \frac{b\Lambda_4}{2} \right] r_0(\mu_c^2, Q^2) + \left[\gamma - \frac{3}{4} \right] r_0(Q_0^2, Q^2) \right),$$
$$\text{for } Q^2 \geq \mu_c^2. \quad (7.3)$$

Next, we take our initial condition (4.16) and use the inverse Mellin transform

$$\int_C \frac{dn}{2\pi i} x^{-n} \frac{e^{y_0 + y_1 n}}{n+1} = x e^{y_0 - y_1} \Theta \left(y_1 + \log \frac{1}{x} \right). \quad (7.4)$$

The condition provided by the theta function means that the formula can be used for $x < \exp(y_1)$. For negative y_1 this means that the validity is limited for x not too close to 1. This, however, has been already tacitly assumed, since the asymptotic expansion holds for fixed values of n, hence cannot describe x in the vicinity of 1. The above formulas lead to the following large-b form of $f_{\text{NS}}^{\text{evol}}$ in the x space:

$$f_{\text{NS}}^{\text{evol}}(x, b, Q) = x \left(\frac{b\Lambda_{\text{QCD}}}{2} \right)^{-8C_F r_0(Q_0^2, Q^2)} \left(\frac{Q}{Q_0} \right)^{-\frac{4C_F}{\beta_0^{(3)}}}$$
$$\times \exp \left(\left[2\gamma - \frac{3}{2} \right] r_0(Q_0^2, Q^2) + \frac{1}{b^3} r_{-3/2}(Q_0^2, Q^2) \right)$$
$$\text{for } Q^2 < \mu_c^2, \quad (7.5)$$

and

$$f_{\text{NS}}^{\text{evol}}(x, b, Q) = x \left(\frac{b}{2} \right)^{-8C_F r_0(Q_0^2, Q^2)} \Lambda_{\text{QCD}}^{-8C_F r_0(Q_0^2, \mu_c^2)}$$
$$\times \Lambda_4^{-8C_F r_0(\mu_c^2, Q^2)} \left(\frac{\mu_c}{Q_0} \right)^{-4C_F/\beta_0^{(3)}} \left(\frac{Q}{\mu_c} \right)^{-4C_F/\beta_0^{(4)}}$$
$$\times \exp \left(\left[2\gamma - \frac{3}{2} \right] r_0(Q_0^2, Q^2) + \frac{1}{b^3} r_{-3/2}(Q_0^2, Q^2) \right)$$
$$\text{for } Q^2 \geq \mu_c^2, \quad (7.6)$$

We note a few facts: the non-singlet UPD of the pion is for large Qb linear in x for x not too close to 1, with the slope decreasing with b as a power law (we can neglect here the small correction due to the last term in Eq. (7.5,7.6). The exponent of b is $-8C_F r_0(Q_0^2, Q^2)$. The overall constant is also determined. Note that linearity with x at not-too-large x is seen in Fig. 2 for the valence quarks (dashed lines) at $b = 10$ GeV^{-1}. Numerically, at $Q = 2$ GeV we find for low x that $f_{\text{NS}}(x, b = 5 \text{ GeV}^{-1}, Q = 2 \text{ GeV}) = 0.73x$ and $f_{\text{NS}}(x, b = 10 \text{ GeV}^{-1}, Q = 2 \text{ GeV}) = 0.35x$, in accordance with the exact calculation of Fig. 2.

The asymptotic form (7.5,7.6) works very efficiently in practice. For the case of the non-singlet quarks this can be seen from Fig. 3, where for $Q = 2$ GeV and $b > 5$ GeV^{-1} there is virtually no difference between the exact numerical calculation and the asymptotic formula.

The power-law behavior in b shows that the evolution generates a rather weak behavior at large b. Numerically, at $Q = 2$, 4, and 100 GeV, the power of b is, respectively, -1.12, -1.29, and -1.75. This means that the large-b behavior for the non-singlet quarks is controlled by the initial profile $F^{\text{NP}}(b)$, which in chiral quark models of the pion has an exponential fall-off, rather than by the QCD evolution.

Now we pass to the discussion of the singlet case of Eq. (3.6). In the large-Qb limit the leading part of the matrix Γ_n of Eq. (3.7) becomes

$$\Gamma_n(Qb) \rightarrow \begin{pmatrix} 4C_F \log \frac{Q^2 b^2}{4} & 0 \\ 0 & 4N_c \log \frac{Q^2 b^2}{4} \end{pmatrix}. \quad (7.7)$$

From this form, using methods as for the non-singlet case above, we infer that the dependence on b is asymptotically

$$f_S(x, b, Q) \sim b^{-8C_F r_0(Q_0^2, Q^2)},$$
$$f_G(x, b, Q) \sim b^{-8N_c r_0(Q_0^2, Q^2)}. \quad (7.8)$$

Thus the singlet quarks fall off at the same rate as the non-singlet quarks of Eq. (7.5,7.6), while the gluons drop significantly faster, as $C_f = 4/3$ and $N_c = 3$. This behavior is clearly seen in Fig. 3. We note that due to the complications of Eq. (3.7) a more detailed analysis yielding pre-factors, such as the one for the non-singlet case presented above, is more difficult in the present case, hence we do not pursue it further here.

We end this section with a couple of remarks concerning the observed long-range nature of the tails in b. Our initial non-perturbative profiles $F^{\mathrm{NP}}(b)$ drop exponentially, therefore suppress the tails generated by the evolution. This means that the large-b, or low-$k_\perp$ behavior is controlled by non-perturbative effects. The larger negative power in f_G, Eq. (7.8), explains the the faster shrinkage of gluon distributions in the b-space, or faster spreading in the $k_\perp$-space.

VIII. BEHAVIOR OF f_{NS} AT $x \to 1$

According to standard properties of the Mellin transform, the limit $x \to 1$ is obtained form the large-n behaviour of the anomalous dimensions. Using the asymptotic form $B(n,m) \to \frac{\Gamma(m)}{n^m}$ in Eq. (C4), or the explicit form of the anomalous dimensions (B6,B7), one obtains that

$$\gamma_{n,NS}(Qb) - \gamma_{n,NS}^{(0)} = 2C_F \frac{b^2 Q^2}{n^2} + \mathcal{O}(1/n^3). \quad (8.1)$$

We also need the large-n expansion of $\gamma_{n,NS}^{(0)}$, which is

$$\gamma_{n,NS}^{(0)} = 8C_F \left(\log n + \gamma - 3/4 + R(n) \right), \quad (8.2)$$

where $R(n) = \sum_{k=1}^{\infty} c_k n^{-k}$. Thus, according to Eq. (3.5), we have the asymptotic form

$$\frac{f_{\mathrm{NS}}^{\mathrm{evol}}(n,b,Q^2)}{f_{\mathrm{NS}}^{\mathrm{evol}}(n,b,Q_0^2)} = n^{-8C_F r_0(Q^2,Q_0^2)} \quad (8.3)$$
$$\times \; e^{-8C_F r_0(\gamma - 3/4 + R(n))} e^{2C_F b^2 r_1/n^2 + \mathcal{O}(1/n^3)}.$$

Using the initial moments (4.16) and expanding the exponentials in Eq. (8.3) we obtain

$$f_{\mathrm{NS}}^{\mathrm{evol}}(n,b,Q^2) = \frac{1}{n+1} n^{-8C_F r_0} \left(1 + \sum_{k=1}^{\infty} c_k' n^{-k} \right)$$
$$\times \; \left(1 + 2C_F b^2 r_1/n^2 + \mathcal{O}(1/n^3) \right). \quad (8.4)$$

Next, we use the formula for the inverse Mellin transform

$$\int_C dn\, x^{-n} \frac{n^{-A}}{n+w} = (-w)^{-A} x^w \left(1 - \frac{\Gamma(A, -w \log \frac{1}{x})}{\Gamma(A)} \right)$$
$$\to \frac{x^w (\log \frac{1}{x})^A}{A \Gamma(A)}, \quad (8.5)$$

which after a straightforward algebra leads to the equation

$$\frac{f_{\mathrm{NS}}^{\mathrm{evol}}(x,b,Q^2)}{f_{\mathrm{NS}}^{\mathrm{evol}}(x,0,Q^2)} = 1 - \frac{2C_F b^2 r_1 (1-x)^2}{(1 + 8C_F r_0)(2 + 8C_F r_0)}$$
$$+ \; \mathcal{O}((1-x)^3). \quad (8.6)$$

The terms with coefficients c_k' do not enter at the leading order in $(1-x)$. The behavior of Eq. (8.6) agrees with the
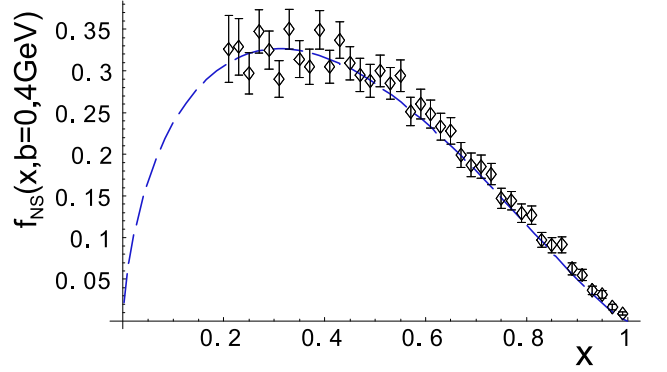

FIG. 5: Model prediction for the *integrated* valence quark distribution of the pion, evolved to from the initial condition (4.16) to the scale of $Q = 4$ GeV, confronted with the E615 Drell-Yan data [58]. The behavior at $x \to 1$ is $(1-x)^{1.29}$.

behaviour of Fig. 2, where close to $x = 1$ the departure of the curves with finite b from the curve with $b = 0$ becomes very slow, as it is suppressed by $(1-x)^2$.

We also obtain that at $x \to 1$ the integrated non-singlet distribution behaves as

$$f_{\mathrm{NS}}(x,0,Q^2) \to \frac{e^{2C_F(3-4\gamma)r_0}}{\Gamma(1 + 8C_F r_0)} (1-x)^{8C_F r_0}. \quad (8.7)$$

This agrees with the fact that a function which originally behaves at $x \to 1$ as $f_{\mathrm{NS}}(x,0,Q_0) \to (1-x)^p$ evolves into [59]

$$f_{\mathrm{NS}}(x,0,Q^2) \to (1-x)^{p - \frac{4C_F}{\beta_0} \log \frac{\alpha(Q)}{\alpha(Q_0)}}. \quad (8.8)$$

In our approach the integrated function at $Q = Q_0$ has $p = 0$. Numerically, we find that

$$f_{\mathrm{NS}}(x,0,(2\text{ GeV})^2) \to 1.15(1-x)^{1.13},$$
$$f_{\mathrm{NS}}(x,0,(4\text{ GeV})^2) \to 1.08(1-x)^{1.29}. \quad (8.9)$$

Note that although with the DGLAP evolution the Brodsky-Lepage counting rules for the behavior at $x \to 1$ are clearly disobeyed, our numerical predictions agree within experimental uncertainties with the experimental data, including the region very close to $x = 1$. Fig. 5 confronts our results evolved to the scale of $Q = 4$ GeV to the E615 experimental Drell-Yan data [58] which cover the large-x region. In view of the simplicity of the present model, the quality of this comparison is impressive.

IX. BEHAVIOR AT $x \to 0$

The low-x behaviour of the inverse Mellin transform is encoded in the closest singularities to the integration line. We start with the non-singlet case of Eq. (3.4). Using the pole-residue expansion of Appendix E we find that the the closest singularity is at $n = -1$, with the

residue $-4C_F J_0(Qb)$. With the help of the expression for the inverse Mellin transform,

$$\int_{-i\infty}^{i\infty} \frac{dn}{2\pi i} \frac{x^{-n}}{n+1} e^{\frac{a}{n+1}} = \begin{cases} xI_0(2\sqrt{a\log\frac{1}{x}}), & a \geq 0 \\ xJ_0(2\sqrt{a\log\frac{1}{x}}), & a < 0 \end{cases}, \quad (9.1)$$

we find that

$$f_{\rm NS}^{\rm evol}(x,b,Q^2) \rightarrow \begin{cases} xI_0(2\sqrt{C_F A\log\frac{1}{x}}), & A \geq 0 \\ xJ_0(2\sqrt{C_F A\log\frac{1}{x}}), & A < 0 \end{cases} \quad (9.2)$$

where

$$A = \int_{Q_0^2}^{Q^2} \frac{dQ^2}{2\pi Q^2} \alpha(Q^2) J_0(Qb). \quad (9.3)$$

For the singlet case we retain the closest singularity at $n = 0$ and rewrite Eq. (3.7) in the form

$$\begin{pmatrix} f_S(n,b,Q) \\ f_G(n,b,Q) \end{pmatrix} = \quad (9.4)$$

$$\exp\left[\int_{Q_0^2}^{Q^2} \frac{dQ'^2 \alpha(Q'^2) J_0(Q'b)}{\pi Q'^2} \begin{pmatrix} 0 & 0 \\ \frac{C_F}{n} & \frac{N_c}{n} \end{pmatrix}\right]$$

$$\times \begin{pmatrix} f_S(n,b,Q_0) \\ f_G(n,b,Q_0) \end{pmatrix},$$

where we have used Eq. (E6), and could drop the $\mathcal{P}$ symbol since in the present approximation the matrix in the exponent does not depend on Q'. After some straightforward algebra we obtain

$$\begin{aligned} f_S(n,b,Q) &= f_S(n,b,Q_0), \\ f_G(n,b,Q) &= f_S(n,b,Q_0)\frac{C_F}{N_c}\left(e^{\frac{2N_cA}{n}} - 1\right) \\ &\quad + f_G(n,b,Q_0)e^{\frac{2N_cA}{n}}. \end{aligned} \quad (9.5)$$

The equation for f_S shows the inadequacy of retaining for this case the singularity at $n = 0$ only, as in the considered limit of $x \to 0$ the singlet quarks are controlled by the singularity at $n = -1$. For the case of gluons we use the initial condition (4.16). We need the inverse Mellin transform

$$\int_C dn x^{-n} \frac{1}{n+1} \exp\left(\frac{a}{n}\right)$$

$$= \sum_{k=0}^{\infty} (-1)^k \left(\frac{\log\frac{1}{x}}{a}\right)^{k/2} I_k(2\sqrt{a\log\frac{1}{x}})$$

$$\sim \frac{\exp\left(2\sqrt{a\log\frac{1}{x}}\right)}{\sqrt{4\pi\sqrt{a\log\frac{1}{x}}\left(1+\sqrt{\frac{\log\frac{1}{x}}{a}}\right)}}, \quad a > 0, \quad (9.6)$$

where in the last line we have used the asymptotic form of the Bessel functions. With this result we find that the unintegrated gluon distribution at $x \to 0$ behaves as

$$f_G(n,b,Q) \sim \exp\left(2\sqrt{2N_cA\log\frac{1}{x}}\right), \quad A > 0, \quad (9.7)$$

with A provided in Eq. (9.3). If $a < 0$ in Eq. (9.6), then the I_k functions above are replaced with the J_k functions, and the asymptotics changes the character from exponential to oscillatory:

$$\begin{aligned} f_G(n,b,Q) &\sim \left[\left(1+\sqrt{\frac{\log\frac{1}{x}}{-A}}\right)\cos\left(2\sqrt{-A\log\frac{1}{x}}\right)\right. \\ &\quad \left. + \left(1-\sqrt{\frac{\log\frac{1}{x}}{-A}}\right)\sin\left(2\sqrt{-A\log\frac{1}{x}}\right)\right] \\ &\quad \times \frac{1}{\sqrt{\pi\sqrt{-A\log\frac{1}{x}}\left(1-\frac{\log\frac{1}{x}}{A}\right)}}, \quad A < 0. \quad (9.8) \end{aligned}$$

For $b = 0$ the result (9.7) is consistent with the double-leading-logarithmic approximation (DLLA) for the DGLAP equation [54], where one obtains, with constant α,

$$xg(x,Q) \sim \exp\left(2\sqrt{\frac{N_c}{\pi}\alpha\log\frac{Q^2}{Q_0^2}\log\frac{1}{x}}\right). \quad (9.9)$$

See, $e.g.$, the review in Ref. [60]. Our formulas (9.2) and (9.7) are generalizations of this behavior for the unintegrated distributions evolved with Eq. (2.4).

The pole-residue expansion of Appendix E is good for not-too-large Qb. This limitation, at any fixed x, carries over to Eq. (9.2) Numerically, we find that at $x = 0.1$ Eq. (9.2) is valid for $Qb \leq 5$. For higher values corrections from further residues should be included.

X. EVOLUTION OF $\langle k_\perp^2 \rangle$

The average transverse momentum squared is a convenient measure of the width of the UPD's. Due to the factorization of the initial profile, Eq. (2.6), $\langle k_\perp^2 \rangle$ decomposes into two terms: the contribution from the initial profile $F^{\rm NP}$, gives the width at the initial scale $Q = Q_0$, and the piece $\langle k_T^2 \rangle_{\rm evol}$, entirely to the evolution and independent of the profile $F^{\rm NP}$,

$$\langle k_\perp^2 \rangle = \langle k_\perp^2 \rangle_{\rm NP} + \langle k_\perp^2 \rangle_{\rm evol}, \quad (10.1)$$

$$\langle k_\perp^2 \rangle_{\rm NP} = -4\left.\frac{dF^{\rm NP}(b)/db^2}{F^{\rm NP}(b)}\right|_{b=0},$$

$$\langle k_\perp^2 \rangle_{\rm evol} = -4\left.\frac{df^{\rm evol}(b,x,Q)/db^2}{f^{\rm evol}(b,x,Q)}\right|_{b=0}.$$

The contribution $\langle k_T^2 \rangle_{\mathrm{NP}}$ has already been discussed in Sec. IV, hence here we analyze the term generated by the evolution.

Let us denote

$$f_j^{(1)}(x,Q) \equiv \left.\frac{df_j^{\mathrm{evol}}(b,x,Q)}{db^2}\right|_{b=0}. \qquad (10.2)$$

In the Mellin space, the equations obtained by expanding Eq. (3.4) up to first order in b^2 around $b=0$ read

$$\frac{df_{\mathrm{NS}}^{(1)}(n,Q)}{dQ^2} = -\frac{\alpha_S(Q^2)}{8\pi Q^2}\left(\gamma_{n,NS}^{(0)}f_{\mathrm{NS}}^{(1)}(n,Q)\right.$$
$$\left. + Q^2\gamma_{n,NS}^{(1)}f_{\mathrm{NS}}(n,0,Q)\right), \qquad (10.3)$$

and

$$\frac{df_S^{(1)}(n,Q)}{dQ^2} = -\frac{\alpha_S(Q^2)}{8\pi Q^2}\left(\gamma_{n,qq}^{(0)}f_S^{(1)}(n,Q)\right.$$
$$+ \gamma_{n,qG}^{(0)}f_G^{(1)}(n,Q)+ \qquad (10.4)$$
$$\left. Q^2[\gamma_{n,qq}^{(1)}f_S(n,0,Q)+\gamma_{n,qG}^{(1)}f_G(n,0,Q)]\right),$$

$$\frac{df_G^{(1)}(n,Q)}{dQ^2} = -\frac{\alpha_S(Q^2)}{8\pi Q^2}\left(\gamma_{n,Gq}^{(0)}f_S^{(1)}(n,Q)\right. \qquad (10.5)$$
$$+ \gamma_{n,GG}^{(0)}f_G^{(1)}(n,Q) +$$
$$\left. Q^2[\gamma_{n,Gq}^{(1)}f_S(n,0,Q)+\gamma_{n,GG}^{(1)}f_G(n,0,Q)]\right),$$

which form a set of ordinary inhomogeneous differential equations. Since at the scale Q_0 all the width is by construction generated by the initial profile F, the initial conditions for Eq. (10.3,10.6) are

$$f_j^{(1)}(n,Q_0) = 0. \qquad (10.6)$$

For the non-singlet case we have the solution

$$f_{\mathrm{NS}}^{(1)}(n,Q) = -\gamma_{n,NS}^{(1)}f_{\mathrm{NS}}(n,0,Q)r_1(Q_0^2,Q^2). \qquad (10.7)$$

In the singlet channel we carry the analysis numerically.

Next, we pass to the x-space via the numerical inverse Mellin transform. The results for the dynamically-generated root mean squared radius of the pion are shown in Fig. 6 for various values of x. In confirmation of the results of Ref. [16], we note that the $k_\perp$ width increases with Q for all parton species. The width for the gluons (solid lines) is larger than the width of the non-singlet (valence) quarks (dashed lines), and the singlet quarks (dotted lines). With the log-log scales of Fig. 6 the slopes of the plotted lines become to a good approximation equal to one another at large Q^2.

With the help of previously-derived expressions for the behaviour of f_{NS} near $x=0$ and $x=1$ we may obtain the following expressions $\langle k_\perp^2 \rangle_{\mathrm{NS}}^{\mathrm{evol}}$ near the end-points. From Eq. (8.8) we have at $x \to 0$

$$\langle k_\perp^2 \rangle_{\mathrm{NS}}^{\mathrm{evol}} \to \frac{I_1(\sqrt{-4C_F r_0 \log x})}{I_0(\sqrt{-4C_F r_0 \log x})}\sqrt{-\frac{C_F \log x}{r_0}}r_1$$
$$\sim \sqrt{-\frac{C_F \log x}{r_0}}r_1. \qquad (10.8)$$

At large Q^2 the leading behavior is

$$\langle k_\perp^2 \rangle_{\mathrm{NS}}^{\mathrm{evol}} \to \sqrt{\frac{2\beta_0^{(4)}C_F \log \frac{1}{x}}{\log \frac{\alpha(\mu_c^2)}{\alpha(Q^2)}}}\frac{\alpha(Q^2)}{8\pi}Q^2, \qquad (10.9)$$

i.e. up to the $\log\log Q^2$ corrections the spreading proceeds with $\alpha(Q^2)Q^2$. At $x \to 1$ we find from Eq. (8.6) that

$$\langle k_\perp^2 \rangle_{\mathrm{NS}}^{\mathrm{evol}} \to \frac{2C_F(1-x)^2 r_1}{(1+8C_F r_0)(2+8C_F r_0)} \qquad (10.10)$$

At large Q^2 the leading behavior is

$$\langle k_\perp^2 \rangle_{\mathrm{NS}}^{\mathrm{evol}} \to \frac{\beta_0^{(4)2}(1-x)^2\alpha(Q^2)}{64\pi C_F \left[\log \frac{\alpha(\mu_c^2)}{\alpha Q^2}\right]^2}Q^2. \qquad (10.11)$$

Again, the growth is, up to the $\log\log Q^2$ corrections, proportional to $\alpha(Q^2)Q^2$.

For the gluons the same asymptotic behavior of $\langle k_\perp^2 \rangle_{\mathrm{G}}^{\mathrm{evol}}$ follows from Eq. (9.6). Thus, to summarize, all UPD's grow at large Q as $Q^2\alpha(Q^2)$, in accordance to the behavior in Fig. 6.

Interestingly, it can be noticed from Fig. 6 that at $Q \to Q_0^+$ the $k_\perp$ width for the gluons does not vanish. In this limit both $f_G^{\mathrm{evol}}(x,0,Q)$ and $f_G^{(1)}(x,Q)$ vanish, as is obvious from Eq. (4.2,10.6). Thus one has a 0/0 limit. From Eq. (2.4,10.3) with the initial condition (4.3,10.6) one can easily obtain that

$$\lim_{Q\to Q_0}\langle k_\perp^2 \rangle_{\mathrm{G}}^{\mathrm{evol}} = Q_0\frac{\int_x^1 dz\, P_{Gq}(z)\frac{(1-z)^2}{z}}{\int_x^1 dz\, P_{Gq}(z)\frac{1}{z}} \qquad (10.12)$$
$$= Q_0\frac{x^4-6x^3+21x^2-18x\log x-10x-6}{3(x^2-2x\log x+x-2)},$$

which is positive for $x \in [0,1)$ and equal 0 for $x=1$. On the other hand, since for the quarks $f_{NS,S}^{\mathrm{evol}}(x,0,Q) \neq 0$ $\langle k_\perp^2 \rangle_{NS,S}^{\mathrm{evol}}$ vanish at Q_0.

In phenomenological applications it is sometimes useful to have a simple formula characterizing the discussed behavior. In the range $2\text{ GeV}^2 < Q^2 < 10000\text{ GeV}^2$ and $0.005 < x < 0.8$ the following simple-minded interpolating formula works to within a few per cent:

$$\left(\langle k_\perp^2 \rangle_i^{\mathrm{evol}}\right)^{1/2} = A_i(\log \frac{1}{x})\left(\frac{Q^2}{\Lambda_{\mathrm{QCD}}^2}\right)^{0.35+0.004\log \frac{Q^2}{\Lambda_{\mathrm{QCD}}^2}},$$
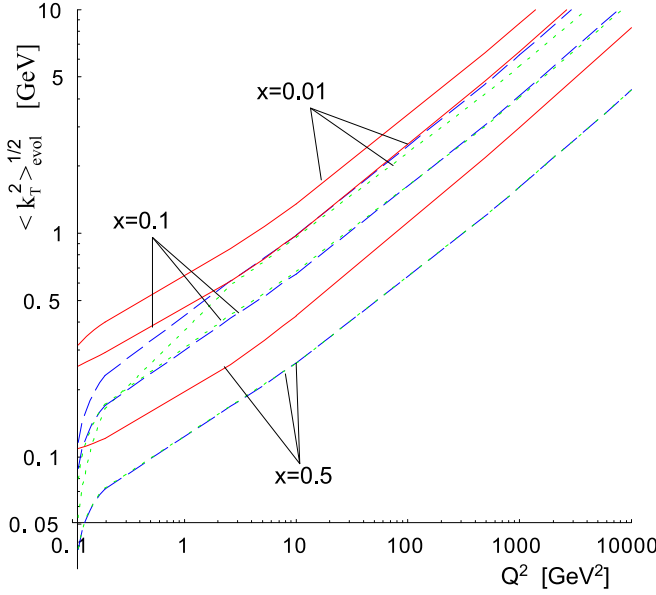
$$(10.13)$$

FIG. 6: The rms transverse momenta of UPD's of the pion for $x = 0.01$, 0.1, and 0.5, plotted as functions of the renormalization scale Q^2. Solid lines – gluons, dashed lines – non-singlet quarks, dotted lines – singlet quarks.

where $i =$NS, S, or G, and

$$
\begin{aligned}
A_{\rm NS}(y) &= -0.017y^{1/2} + 0.113y - 0.057y^{3/2} + 0.010y^2, \\
A_S(y) &= -0.021y^{1/2} + 0.120y - 0.059y^{3/2} + 0.009y^2, \\
A_G(y) &= -0.016y^{1/2} + 0.150y - 0.075y^{3/2} + 0.011y^2.
\end{aligned}
\tag{10.14}
$$

The power of Q^2 of 0.35 in Eq. (10.13), rather than $1/2$ corresponding to $\langle k_\perp^2 \rangle_i^{\rm evol} \sim Q^2 \alpha(Q^2)$, compensates, in the chosen range for Q, for the logarithmic corrections. We note that Eq. (10.13) holds for the pion with the initial conditions (4.16) provided by the chiral quark models.

XI. FORMAL LIMITS FOR OTHER INITIAL CONDITIONS

Certain formal results listed in this paper, such as the formulas for the non-singlet quarks, (7.5, 7.6, 8.7, 8.8, 9.2, 10.8,10.9), are specific to the evolution with the initial condition following from the chiral quark models, Eq. (4.4, 4.16). However, these results can be easily generalized. Note that most of the popular parameterizations of initial conditions, such as those of Refs. [52, 53], involve linear combinations of $x^\alpha(1-x)^\beta$. It is understood that the factorization in the initial condition between x and b variable holds, as assumed in Ref. [16].

For the case of large-b asymptotics, the relevant formula is (7.4). With the initial condition $x^\alpha(1-x)^\beta$ it

becomes

$$
\int_C \frac{dn}{2\pi i} x^{-n} \frac{e^{y_0 + y_1 n}}{n + \alpha} = x^\alpha e^{y_0 - \alpha y_1} \Theta\left(y_1 + \log\frac{1}{x}\right) (11.1)
$$

and expressions (7.5,7.6) are modified accordingly, with x replaced by x^α, and y_1 in the exponent multiplied by α. The formulas (7.8) remain valid. Therefore the power-law behavior at large b is independent of the initial condition, and is $b^{-8C_F r_0(Q_0^2, Q^2)}$ for the quarks and $b^{-8N_c r_0(Q_0^2, Q^2)}$ for the gluons.

In the limit of $x \to 1$ the only difference is the appearance of the extra power of β in the in Eq. (8.7). Thus, the UPD's for finite b approach the $b = 0$ case of the integrated distributions as $(1-x)^2$.

In the limit of $x \to 0$ we need generalizations of the Mellin transforms of Eq. (9.1,9.6) for $\alpha \neq 1$. These are

$$
\int_C dn\, x^{-n} \frac{1}{n + \alpha} \exp\left(\frac{a}{n+1}\right) \tag{11.2}
$$

$$
= x \sum_{k=0}^{\infty} (-1)^k (\alpha - 1)^k \left(\frac{\log\frac{1}{x}}{a}\right)^{k/2} I_k\left(2\sqrt{a\log\frac{1}{x}}\right)
$$

$$
\sim \frac{x \exp\left(2\sqrt{a\log\frac{1}{x}}\right)}{(\alpha - 1)\sqrt{4\pi\sqrt{a\log\frac{1}{x}}}\sqrt{\frac{\log\frac{1}{x}}{a}}}, \quad \alpha \neq 1,\ a > 0,
$$

and

$$
\int_C dn\, x^{-n} \frac{1}{n + \alpha} \exp\left(\frac{a}{n}\right) \tag{11.3}
$$

$$
= \sum_{k=0}^{\infty} (-1)^k \alpha^k \left(\frac{\log\frac{1}{x}}{a}\right)^{k/2} I_k\left(2\sqrt{a\log\frac{1}{x}}\right)
$$

$$
\sim \frac{\exp\left(2\sqrt{a\log\frac{1}{x}}\right)}{\alpha\sqrt{4\pi\sqrt{a\log\frac{1}{x}}}\sqrt{\frac{\log\frac{1}{x}}{a}}}, \quad \alpha \neq 0,\ a > 0.
$$

The analogs of Eq. (9.2,9.7,10.8,10.9) follow straightforwardly. In particular, the $Q^2\alpha(Q^2)$ large-Q behavior for all parton distributions is preserved.

XII. CONCLUSIONS

We have presented a new method of solving the Kwieciński equations for the leading-order QCD evolution of unintegrated parton distributions. The method is based on the Mellin transform and parallels the standard analysis of the DGLAP equations. Our main results are as follows:

1. We have found analytic forms of the b-dependent anomalous dimensions, expressed through hypergeometric functions, which allowed us to study formal aspects of the equations and their solutions, *e.g.* the asymptotic forms of the evolution-generated

UPD's at large b, or at $x \to 0$ and $x \to 1$. We have also demonstrated that the proposed numerical method is fast and stable.

2. The numerical work can be simplified if low-b or large-b expansions are used.

3. At large b the evolution-generated b-dependent UPD's exhibit power-law fall-off, with the magnitude of the exponents growing with the probing scale Q, *cf.* Eq. (7.5,7.8). The fall-off is steeper for the gluons than for the quarks.

4. At $x \to 0$ we have found generalizations of the DLLA behavior, *cf.* Eq. (9.2,9.7.) We have also shown that for large b the solution for the valence UPD of the pion grows linearly with x for not too large x, and the slope decreases with b as a power law.

5. At $x \to 1$ the evolution-generated b-dependent UPD's approach the integrated distributions as $(1-x)^2$.

6. Our numerical results fully confirm the finding of Ref. [16], where a different numerical method was used. We find the spreading of the $k_\perp$ distributions with the probing scale Q, with the effect strongest for gluons and increasing with decreasing x. We have also shown that the widths $\langle k_\perp^2 \rangle_i^{\text{evol}}$ in all channels i increase at large Q^2 as $Q^2 \alpha(Q^2)$.

7. For practical purposes in possible phenomenological applications, we have parameterized $\langle k_\perp^2 \rangle_i^{evol}$ with a simple formula which works with accuracy of a few percent.

Although the specific study of this paper was devoted to the pion with the initial condition following from the chiral models, and several of the more detailed analytic formulas were specific to this case, the developed method is general and can be applied to any initial form of the data. In particular, it can be used with the GRS [52] or GRV [53] parameterization supplied by a profile in b, such as already studied in Ref. [16]. The formal results of Sec. XI are general for a wide class of initial conditions, suitable for both the pion and the nucleon.

Acknowledgments

APPENDIX A: ELEMENTS OF THE PERTURBATIVE QCD EVOLUTION

We use the LO QCD evolution with three active flavors up to the scale $\mu_c^2 = 4 \text{ GeV}^2$ and four active flavors above. Therefore $\alpha = g^2/(4\pi)$ is given by

$$\alpha(Q^2) = \frac{4\pi}{\beta_0^{(3)} \log\left(\frac{Q^2}{\Lambda_{QCD}^2}\right)}, \qquad Q^2 \leq \mu_c^2,$$

$$\alpha(Q^2) = \frac{4\pi}{\beta_0^{(4)} \log\left(\frac{Q^2}{\Lambda_4^2}\right)}, \qquad Q^2 > \mu_c^2,$$

$$\Lambda_4 = \mu_c \left(\frac{\Lambda_{QCD}}{\mu_c}\right)^{\frac{\beta_0^{(3)}}{\beta_0^{(4)}}}, \qquad (A1)$$

with $\beta_0^{(N_f)} = 11 - 2N_f/3$ for $N_c = 3$, where N_f and N_c denote the number of flavors and colors, respectively. Along this paper we take

$$\Lambda_{\text{QCD}} = 226 \text{ MeV}, \qquad (A2)$$

as was done in Refs. [42, 45, 46, 47]. The value of the scale Λ_4 ensures matching at $Q^2 = \mu_c^2$. Numerically, $\beta_0^{(3)} = 9$, $\beta_0^{(4)} = 25/3$, and $\Lambda_4 = 189$ MeV.

The functions r_k, defined in Eq. (A), have the explicit form

$$r_0(Q_0^2, Q^2) = \frac{1}{2\beta_0^{(3)}} \log\left(\frac{\log(Q^2/\Lambda_{\text{QCD}}^2)}{\log(Q_0^2/\Lambda_{\text{QCD}}^2)}\right)$$

$$= \frac{1}{2\beta_0^{(3)}} \log \frac{\alpha(Q_0^2)}{\alpha(Q^2)}, \qquad Q^2 \leq \mu_c^2,$$

$$r_0(Q_0^2, Q^2) = r_0(Q_0^2, \mu_c^2) + \frac{1}{2\beta_0^{(4)}} \log\left(\frac{\log(Q^2/\Lambda_4^2)}{\log(\mu_c^2/\Lambda_4^2)}\right)$$

$$= r_0(Q_0^2, \mu_c^2) + \frac{1}{2\beta_0^{(4)}} \log \frac{\alpha(\mu_c^2)}{\alpha(Q^2)}, \qquad (A3)$$

$$Q^2 > \mu_c^2,$$

and for $k \neq 0$

$$r_k(Q_0^2, Q^2) = \frac{\Lambda_{\text{QCD}}^{2k}}{2\beta_0^{(3)}} \left[\text{Li}\left(\frac{Q^{2k}}{\Lambda_{\text{QCD}}^{2k}}\right) - \text{Li}\left(\frac{Q_0^2}{\Lambda_{\text{QCD}}^{2k}}\right)\right],$$

$$Q^2 \leq \mu_c^2,$$

$$r_k(Q_0^2, Q^2) = r_k(Q_0^2, \mu_c^2) + \frac{\Lambda_4^{2k}}{2\beta_0^{(4)}} \qquad (A4)$$

$$\times \left[\text{Li}\left(\frac{Q^{2k}}{\Lambda_4^{2k}}\right) - \text{Li}\left(\frac{\mu_c^2}{\Lambda_4^2}\right)\right], \qquad Q^2 > \mu_c^2.$$

Above we have used the indefinite integral

$$\int \frac{dQ^2 Q^{2k}}{Q^2 \log(Q^2/\Lambda^2)} = \Lambda^{2k} \mathrm{Li}\left(\frac{Q^{2k}}{\Lambda^{2k}}\right), \quad k = 1, 2, \ldots, \tag{A5}$$

where the logarithmic integral is

$$\mathrm{Li}(x) = \int_0^x dt/\log t. \tag{A6}$$

At large Q^2

$$\Lambda^{2k} \mathrm{Li}\left(\frac{Q^{2k}}{\Lambda^{2k}}\right) = Q^{2k}\left(\frac{1}{k \log \frac{Q^2}{\Lambda^2}} + \frac{1}{k^2 \log^2 \frac{Q^2}{\Lambda^2}} + \ldots\right). \tag{A7}$$

The functions $P_{ab}(z)$ are the LO splitting functions corresponding to real emission, *i.e.*:

$$P_{qq}(z) = C_F \frac{1+z^2}{1-z}, \tag{A8}$$
$$P_{qG}(z) = N_f[z^2 + (1-z)^2],$$
$$P_{Gq}(z) = C_F \frac{1+(1-z)^2}{z},$$
$$P_{GG}(z) = 2N_c\left[\frac{z}{1-z} + \frac{1-z}{z} + z(1-z)\right],$$

with $C_F = (N_c^2 - 1)/(2N_c) = 4/3$.

APPENDIX B: b-DEPENDENT ANOMALOUS DIMENSIONS

We introduce

$$u = \frac{Q^2 b^2}{4}, \tag{B1}$$

as well as the anomalous dimensions for the $b = 0$ case of the DGLAP equations, where for the non-singlet we have

$$\gamma_{n,NS}^{(0)} = 2C_F\left(-3 + \frac{2}{1+n} + \frac{2}{2+n} + 4H_n\right), \tag{B2}$$

while for the singlet

$$\gamma_{n,qq}^{(0)} = \gamma_{n,NS}(0), \tag{B3}$$
$$\gamma_{n,qG}^{(0)} = -4N_f\left(\frac{1}{1+n} - \frac{2}{2+n} + \frac{2}{3+n}\right),$$
$$\gamma_{n,Gq}^{(0)} = -4C_F\left(\frac{2}{n} - \frac{2}{1+n} + \frac{1}{2+n}\right),$$
$$\gamma_{n,GG}^{(0)} = 2N_c\left(-3 - \frac{4}{n} + \frac{8}{1+n} - \frac{4}{2+n} + \frac{4}{3+n} + 4H_n\right).$$

The symbol H_n denotes the harmonic number

$$H_n = \sum_{k=1}^n \frac{1}{k} = \frac{\Gamma'(n+1)}{\Gamma(n+1)} + \gamma, \tag{B4}$$

which is a meromorphic function in the complex n variable, with poles located at negative integers $n = -1, -2, -3, \ldots$ and residues equal to -1.

Below we list the anomalous dimensions for the moments of the unintegrated parton distributions in the b space, defined in Eq. (3.2). The formulas follow from the basic analytic integral

$$\frac{\Gamma(2+\mu+\nu)}{\Gamma(1+\mu)\,\Gamma(1+\nu)} \int_0^1 dy\, y^\mu (1-y)^\nu J_0\left(2\sqrt{uy}\right) =$$
$$_2F_3\left(\frac{1+\mu}{2}, \frac{2+\mu}{2}; 1, \frac{2+\mu+\nu}{2}, \frac{3+\mu+\nu}{2}; -u\right) \tag{B5}$$

and relations among the generalized hypergeometric functions. For the non-singlet case we have

$$\gamma_{n,NS}(Qb) = \gamma_{n,NS}^{(0)} + \frac{4C_F}{(1+n)(2+n)}\left[-3 - 2n + 2(2+n)\,_1F_2(\frac{1}{2}; \frac{2+n}{2}, \frac{3+n}{2}; -u)\right.$$
$$\left. - \,_1F_2(\frac{3}{2}; \frac{3+n}{2}, \frac{4+n}{2}; -u) + 2u\,_3F_4(1, 1, \frac{3}{2}; 2, 2, \frac{3+n}{2}, \frac{4+n}{2}; -u)\right], \tag{B6}$$

whereas for the singlet case

$$\gamma_{n,qq}(Qb) = \gamma_{n,NS}(Qb),$$

$$\gamma_{n,qG}(Qb) = \gamma_{n,qG}^{(0)} + \frac{4N_f}{(1+n)(2+n)(3+n)(4+n)(5+n)} \left[-\left((4+n)(5+n)(-4-n(3+n)) \right. \right.$$
$$+ (2+n)(3+n) \, _2F_1(\tfrac{1}{2}; \tfrac{2+n}{2}, \tfrac{3+n}{2}; -u) - 2(3+n) \, _1F_2(\tfrac{3}{2}; \tfrac{3+n}{2}, \tfrac{4+n}{2}; -u)$$
$$\left. \left. + 4 \, _1F_2(\tfrac{3}{2}; \tfrac{4+n}{2}, \tfrac{5+n}{2}; -u) \right) \right) + 24 \, u \, _1F_2(\tfrac{5}{2}; \tfrac{6+n}{2}, \tfrac{7+n}{2}; -u) \right],$$

$$\gamma_{n,Gq}(Qb) = \gamma_{n,Gq}^{(0)} + \frac{4C_F}{n(1+n)(2+n)(3+n)(4+n)}$$
$$\times \left[-\left((1+n)(2+n)(3+n)(4+n) \, _1F_2(\tfrac{1}{2}; \tfrac{1+n}{2}, \tfrac{2+n}{2}; -u) \right) \right.$$
$$\left. + (3+n)(4+n) \left(4+n(3+n) - 2 \, _1F_2(\tfrac{3}{2}; \tfrac{3+n}{2}, \tfrac{4+n}{2}; -u) \right) + 12 \, u \, _1F_2(\tfrac{5}{2}; \tfrac{5+n}{2}, \tfrac{6+n}{2}; -u) \right],$$

$$\gamma_{n,GG}(Qb) = \gamma_{n,GG}^{(0)} + 8N_c \left[\frac{1}{n} - \frac{2}{1+n} + \frac{1}{2+n} - \frac{1}{3+n} + \frac{_1F_2(\tfrac{1}{2}; 1+\tfrac{n}{2}, \tfrac{3}{2}+\tfrac{n}{2}; -u)}{1+n} - \frac{_1F_2(\tfrac{3}{2}; 1+\tfrac{n}{2}, \tfrac{3}{2}+\tfrac{n}{2}; -u)}{n+n^2} \right.$$
$$- \frac{_1F_2(\tfrac{3}{2}; \tfrac{3}{2}+\tfrac{n}{2}, 2+\tfrac{n}{2}; -u)}{(1+n)(2+n)} + \frac{2 \, _1F_2(\tfrac{3}{2}; 2+\tfrac{n}{2}, \tfrac{5}{2}+\tfrac{n}{2}; -u)}{(1+n)(2+n)(3+n)} - \frac{12 \, u \, _1F_2(\tfrac{5}{2}; 3+\tfrac{n}{2}, \tfrac{7}{2}+\tfrac{n}{2}; -u)}{(1+n)(2+n)(3+n)(4+n)(5+n)}$$
$$\left. + \frac{u \, _3F_4(1, 1, \tfrac{3}{2}; 2, 2, \tfrac{3}{2}+\tfrac{n}{2}, 2+\tfrac{n}{2}; -u)}{(1+n)(2+n)} \right]. \tag{B7}$$

One may verify that the analyticity properties in n of the anomalous dimensions (B6,B7) are the same as for the $b=0$ case of (B2,B4).

APPENDIX C: EXPANSION OF ANOMALOUS DIMENSIONS AT LOW bQ

We may expand in the anomalous dimensions in powers of $Q^2 b^2$,

$$\gamma_{n,j}(Qb) = \gamma_{n,j}^{(0)} + \gamma_{n,j}^{(1)} Q^2 b^2 + \dots, \tag{C1}$$

which yields

$$\gamma_{n,NS}^{(1)} = \gamma_{n,qq}^{(1)} = \frac{2C_F(n^2 + 5n + 7)}{(n+1)(n+2)(n+3)(n+4)},$$
$$\gamma_{n,qG}^{(1)} = \frac{2N_f(n^2 + 3n + 14)}{(n+1)(n+2)(n+3)(n+4)},$$
$$\gamma_{n,Gq}^{(1)} = \frac{2C_F(n^2 + 7n + 24)}{(n+1)(n+2)(n+3)(n+4)},$$
$$\gamma_{n,GG}^{(1)} = \frac{2N_c[n(n+5)(n^2 + 5n + 16) + 120]}{n(n+1)n+2)(n+3)(n+4)(n+5)}. \tag{C2}$$

More generally, introducing the Euler Beta function, $\mathsf{B}(x,y) = \Gamma(x)\Gamma(y)/\Gamma(x+y)$, and applying the series expansion of the Bessel function,

$$J_0(x) = \sum_{k=0}^{\infty} \frac{(-x^2)^k}{2^k k!^2}, \tag{C3}$$

we arrive at the expansion formulas

$$\gamma_{n,NS}(Qb) = \gamma_{n,qq}(Qb) = \gamma_{n,qq}^{(0)}$$
$$- C_F \sum_{k=1}^{\infty} \frac{(-Q^2 b^2)^k 4^{1-k}}{k!^2} [\mathsf{B}(2k, n+1) + \mathsf{B}(2k, n+3)]$$

$$\gamma_{n,qG}(Qb) = \gamma_{n,qG}^{(0)} - N_f \sum_{k=1}^{\infty} \frac{(-Q^2 b^2)^k 4^{1-k}}{k!^2}$$
$$\times [\mathsf{B}(2k+1, n+1) - 2\mathsf{B}(2k+1, n+2)$$
$$+ 2\mathsf{B}(2k+1, n+3)]$$

$$\gamma_{n,Gq}(Qb) = \gamma_{n,Gq}^{(0)} - C_F \sum_{k=1}^{\infty} \frac{(-Q^2 b^2)^k 4^{1-k}}{k!^2}$$
$$\times [2\mathsf{B}(2k+1, n) - 2\mathsf{B}(2k+1, n+1)$$
$$+ \mathsf{B}(2k+1, n+2)] \tag{C4}$$

$$\gamma_{n,GG}(Qb) = \gamma_{n,GG}^{(0)} - 2N_c \sum_{k=1}^{\infty} \frac{(-Q^2 b^2)^k 4^{1-k}}{k!^2}$$
$$\times [\mathsf{B}(2k, n+2) + \mathsf{B}(2k+2, n) + \mathsf{B}(2k+2, n+2)].$$

APPENDIX D: ASYMPTOTICS OF THE ANOMALOUS DIMENSIONS AT LARGE bQ

We may use the asymptotic forms of the generalized hypergeometric functions appearing in Eq. (B6,B7). One

has [62]

$$
{}_1F_2(a_1; b_1, b_2; -\frac{Q^2 b^2}{4}) = \frac{\Gamma(b_1)\Gamma(b_2)}{\Gamma(b_1-a_1)\Gamma(b_2-a_1)}\left(\frac{4}{Q^2 b^2}\right)^{a_1}
$$

$$
+\frac{\Gamma(b_1)\Gamma(b_2)}{\sqrt{\pi}\Gamma(a_1)}\{\cos(Qb - \pi c_1)
$$

$$
+\frac{c_2}{Qb}\sin(Qb - \pi c_1)\}\left(\frac{4}{Q^2 b^2}\right)^{c_1} + \dots,
$$

$$
c_1 = \frac{1}{2}\left(b_1 + b_2 - a_1 - \frac{1}{2}\right), \tag{D1}
$$

$$
c_2 = \frac{1}{8}\left(12a_1^2 - 8(b_1 + b_2 + 1)a_1 - 4(b_1 - b_2)^2\right.
$$

$$
\left. +8(b_1 + b_2) - 3\right),
$$

and [63]

$$
{}_3F_4\left(1, 1, \frac{3}{2}; 2, 2, \frac{n+3}{2}, \frac{n+4}{2}; -\frac{Q^2 b^2}{4}\right) =
$$

$$
\frac{4(n+1)(n+2)}{nQ^3 b^3}\left(Qb[n\log\frac{Qb}{2} - n\psi^0(n) - 1] + n^2\right)
$$

$$
+\frac{8\Gamma(n+3)}{\sqrt{2\pi}}\cos\left(Qb - \frac{2n+3}{4}\pi\right)(Qb)^{-\frac{n}{2}-\frac{7}{2}} + \dots
\tag{D2}
$$

Then the following asymptotic expansions for the b-dependent anomalous dimensions hold:

$$
\gamma_{\mathrm{NS}}(n, Qb) = \gamma_{qq}(n, Qb) = 4C_F\left(\log\frac{Q^2 b^2}{4} + 2\gamma - \frac{3}{2}\right.
$$

$$
+\frac{2n+2}{Qb} + \frac{\Gamma(n+1)(Qb)^{-n-\frac{5}{2}}}{4\sqrt{2\pi}}
$$

$$
\times\left[24bQ\cos(\frac{2n+3}{4}\pi - Qb)\right.
$$

$$
\left.\left. -(12n+13)\sin(\frac{2n+3}{4}\pi - Qb)\right]\right) + \dots
\tag{D3}
$$

$$
\gamma_{qG}(n, Qb) = 4N_f\left(-\frac{1}{Qb} + \frac{\Gamma(n+1)(Qb)^{-n-\frac{5}{2}}}{8\sqrt{\pi}}\right.
$$

$$
\times\left[(-12n+8Qb-11)\cos(\frac{n\pi}{2} - Qb)\right.
$$

$$
\left.\left. +(12n+8Qb+11)\sin(\frac{n\pi}{2} - Qb)\right]\right) + \dots
\tag{D4}
$$

$$
\gamma_{Gq}(n, Qb) = 4C_F\left(-\frac{1}{Qb} + \frac{\Gamma(n)(Qb)^{-n-\frac{3}{2}}}{4\sqrt{\pi}}\right.
$$

$$
\times\left[(4n+8Qb-1)\cos(\frac{n\pi}{2} - Qb)\right.
$$

$$
\left.\left. +(4n-8Qb-1)\sin(\frac{n\pi}{2} - Qb)\right]\right) + \dots
\tag{D5}
$$

$$
\gamma_{GG}(n, Qb) = \frac{4N_f}{3} + 4N_c\left(\log\frac{Q^2 b^2}{4} + 2\gamma - \frac{11}{6}\right.
$$

$$
+\frac{2n+2}{Qb} - \frac{4\Gamma(n)(Qb)^{-n-\frac{1}{2}}}{\sqrt{2\pi}}\cos(\frac{2n+1}{4}\pi - Qb)
$$

$$
+\frac{[\Gamma(n) - 20\Gamma(n+1)](Qb)^{-n-\frac{3}{2}}}{4\sqrt{\pi}}
$$

$$
\left.\times[\cos(\frac{n}{2}\pi - Qb) + \sin(\frac{n}{2}\pi - Qb)]\right) + \dots
\tag{D6}
$$

The ellipses denote terms subleading in $\frac{1}{Qb}$. The above formulas assume that n is kept fixed. In actual applications, such as numerical programming of the generalized hypergeometric functions, it is practical to switch from the general formulas (B6,B7) to the asymptotic expressions (D3,D6) when $Qb \geq 10|n|$.

APPENDIX E: POLE-RESIDUE EXPANSION OF THE ANOMALOUS DIMENSIONS

For $b \neq 0$ the analytic structure of the b-dependent anomalous dimensions remains the same as for $b = 0$. This can be seen by expanding the Bessel function in the integrand of Eq. (3.2) as a power series around $z = 0$, which yields

$$
\gamma_{n,ab}(Qb) = \tag{E1}
$$

$$
-4\int_0^1 dz \sum_{k=0}^{\infty}\frac{1}{k!}\left[J_0^{(k)}(Qb)(-Qb)^k z^{n+k} - 1\right]P_{ab}(z).
$$

Applying the trick

$$
1 = J_0(0) = -4\sum_{k=0}^{\infty}\frac{1}{k!}J_0^{(k)}(Qb)(-Qb)^k, \tag{E2}
$$

we find the expansion involving index-shifted anomalous dimensions at $b = 0$, namely

$$
\gamma_{n,ab}(Qb) = \sum_{k=0}^{\infty}\frac{(-Qb)^k}{k!}J_0^{(k)}(Qb)\gamma_{n+k,ab}(0).
\tag{E3}
$$

Using the explicit expression for the anomalous dimension this series may be rewritten as a pole-residue expansion

$$
\gamma_{n,ab}(Qb) = \sum_{k=0}^{\infty}\frac{R_k^{ab}(Qb)}{n+k}. \tag{E4}
$$

In practice this means that the Mellin contour used in the case of $b = 0$ can be used in the $b \neq 0$ case as well. In the non-singlet case the first few residues read

$$
R_1^{\mathrm{NS}}(A) = -4C_F J_0(A), \tag{E5}
$$

$$
R_2^{\mathrm{NS}}(A) = -4C_F(J_0(A) + AJ_1(A)),
$$

$$
R_3^{\mathrm{NS}}(A) = -2C_F(-(A^2 - 4)J_0(A) + 3AJ_1(A)),
$$

while in the singlet channel $R_i^{qq} = R_i^{\text{NS}}$ and

$$
\begin{aligned}
R_1^{qG}(A) &= -4N_F J_0(A), \\
R_2^{qG}(A) &= -4N_F(-2J_0(A) + AJ_1(A)), \\
&\quad \ldots \\
R_0^{Gq}(A) &= -8C_F J_0(A), \\
R_1^{Gq}(A) &= -8C_F(-J_0(A) + AJ_1(A)), \\
&\quad \ldots \\
R_0^{GG}(A) &= -8N_c J_0(A), \\
R_1^{GG}(A) &= -8N_c(-J_0(A) + AJ_1(A)). \qquad \text{(E6)}
\end{aligned}
$$

The pole-residue expansion controls the behavior of the solutions of Eq. (2.4) at low x. Since the subsequent residues carry powers of $A^n = (Qb)^n$, the expansion cannot be used for Qb too large.

[1] Yu. L. Dokshitzer, D. I. Dyakonov and S. I. Troyan, Phys. Rep. **58** (1980) 269.
[2] N. Nakamura, G. Pancheri and Y.N. Srivastava, Z. Phys. **C21** (1984) 243; A. Corsetti, A. Grau, G. Pancheri, Y.N. Srivastava Phys. Lett. **B382** (1996) 282; A. Grau, G. Pancheri, Y.N. Srivastava, Phys. Rev. **D60** (1999) 114020.
[3] G. Sterman, *Partons, factorization and resummation TASI 95*, based on seven lectures at the Theoretical Advanced Study Intitute, *QCD and beyond*, Boulder, Colorado, June 1995, hep-ph/9606312.
[4] M. A. Kimber, A. D. Martin and M. G. Ryskin, Eur. Phys. J. C **12**, 655 (2000).
[5] M. A. Kimber, A. D. Martin, J. Kwieciński and A. M. Staśto, Phys. Rev. **D62** (2000) 094006.
[6] M. A. Kimber, A. D. Martin and M. G. Ryskin, Phys. Rev. D **63**, 114027 (2001).
[7] A. D. Martin and M. G. Ryskin, Phys. Rev. **D64** (2001) 094017.
[8] V. A. Khoze, A. D. Martin and M. G. Ryskin, Eur. Phys. J. **C14** (2000) 525; *ibid.* **C19** (2001) 477; Erratum - *ibid.* **C20** (2001) 599.
[9] G. Watt, A. D. Martin and M. G. Ryskin, hep-ph/0306169.
[10] G. Gustafson, L. Lönnblad and G. Miu, JHEP **0209** (2002)005.
[11] J. C. Collins, Acta Phys. Polon. **B34** (2003) 3103.
[12] A. Szczurek, Acta Phys. Polon. **B34** (2003) 3191.
[13] A. D. Martin and M. G. Ryskin, Phys. Rev. D **64**, 094017 (2001).
[14] J. Kwieciński, Acta Phys. Polon. B **33**, 1809 (2002).
[15] A. Gawron and J. Kwieciński, Acta Phys. Polon. B **34** (2003) 133.
[16] A. Gawron, J. Kwieciński and W. Broniowski, Phys. Rev. D **68**, 054001 (2003).
[17] M. Ciafaloni, *Nucl. Phys.* **B 296**(1988) 49.
[18] S. Catani, F. Fiorani, G. Marchesini, *Phys. Lett.* **B 234**(1990)339.
[19] S. Catani, F. Fiorani, G. Marchesini, *Nucl. Phys.* **B 336**(1990)18.
[20] G. Marchesini, *Nucl. Phys.* **B 445**(1995) 49.
[21] H. Jung, Mod. Phys. Lett. A **19**, 1 (2004).
[22] A. Gawron and J. Kwiecinski, arXiv:hep-ph/0309303.
[23] J. Kwieciński and A. Szczurek, Nucl. Phys. B **680**, 164 (2004).
[24] M. Hansson, H. Jung and L. Jonsson, arXiv:hep-ph/0402019.
[25] L. Motyka and N. Timneanu, Eur. Phys. J. C **27** (2003) 73.
[26] N. P. Zotov, A. V. Lipatov and V. A. Saleev, Phys. Atom. Nucl. **66**, 755 (2003) [Yad. Fiz. **66**, 786 (2003)].
[27] A. V. Lipatov and N. P. Zotov, arXiv:hep-ph/0304181.
[28] G. Watt, A. D. Martin and M. G. Ryskin, Eur. Phys. J. C **31**, 73 (2003).
[29] A. Szczurek, arXiv:hep-ph/0311175.
[30] T. S. Biro and B. Muller, Phys. Lett. B **578**, 78 (2004).
[31] P. Levai, G. Papp, G. G. Barnafoldi and G. Fai, arXiv:nucl-th/0306019.
[32] A. V. Kotikov, A. V. Lipatov and N. P. Zotov, arXiv:hep-ph/0403135.
[33] A. V. Kotikov, A. V. Lipatov, G. Parente and N. P. Zotov, Eur. Phys. J. C **26**, 51 (2002).
[34] J. Kwieciński and B. Ziaja, Phys. Rev. D **60**, 054004 (1999)
[35] J. Kwiecinski and B. Ziaja, Phys. Rev. D **63**, 054022 (2001)
[36] A. I. Shoshi, F. D. Steffen, H. G. Dosch and H. J. Pirner, Phys. Rev. D **66**, 094019 (2002).
[37] V. Gribov, L. Lipatov, *Sov. J. Nucl. Phys.* **15**(1972)438; *ibid.* 675.
[38] L. Lipatov, *Sov. J. Nucl. Phys.* **20**(1975)94.
[39] G. Altarelli, G. Parisi, *Nucl. Phys.* **B 126**(1977)298.
[40] Y. Dokshitser, *Sov. Phys. JETP* **46**(1977)641.
[41] E. Ruiz Arriola, proc. of Workshop on *Lepton Scattering, Hadrons and QCD*, Adelaide (Australia), 26 March – 6 April 2001. Eds. W. Melnitchouk, A. W. Schreiber, A. W. Thomas, P. C. Tandy, Singapore, World Scientific, 2001, hep-ph/0107087.
[42] E. Ruiz Arriola and W. Broniowski, Phys. Rev. D **67**, 074021 (2003).
[43] E. Ruiz Arriola and W. Broniowski, proc. of *Light cone physics: Hadrons and beyond*, IPPP, University of Durham, UK, 5-9 August 2003, ed. S. Dalley, p. 166, arXiv:hep-ph/0310044.
[44] For reviews see, e.g., U. Vogl and W. Weise, *Progress in Particle and Nuclear Physics* vol. **27**, 195 (1991); S. P. Klevansky, Rev. Mod. Phys. **64**, 649 (1992); M. K. Volkov, Part. and Nuclei B 24, 1 (1993); T. Hatsuda and T. Kunihiro, Phys. Rep. **247**, 221 (1994); Chr. V. Christov, A. Blotz, H.-C. Kim, P. Pobylitsa, T. Watabe, T. Meissner, E. Ruiz Arriola, and K. Goeke, Prog. Part. Nucl. Phys. **37**, 91 (1996); R. Alkofer, H. Reinhardt,

and H. Weigel, Phys. Rept. **265**, 139 (1996); G. Ripka, *Quarks Bound by Chiral Fields* Oxford Science Publications, 1997, and references therein.

[45] R. M. Davidson and E. Ruiz Arriola, Acta Phys. Polon. B **33**, 1791 (2002).

[46] R. M. Davidson and E. Ruiz Arriola, Phys. Lett. B **348**, 163 (1995).

[47] H. Weigel, E. Ruiz Arriola and L. P. Gamberg, Nucl. Phys. B **560**, 383 (1999).

[48] E. Ruiz Arriola, Acta Phys. Polon. B **33**, 4443 (2002).

[49] E. Ruiz Arriola and W. Broniowski, Phys. Rev. D **66**, 094016 (2002).

[50] W. Broniowski and E. Ruiz Arriola, Phys. Lett. B **574**, 57 (2003).

[51] L. Theußel, S. Noguera, and V. Vento, arXiv:nucl-th/0211036.

[52] M. Glück, E. Reya, I. Schienbein, Eur. Phys. J. **C10**, 313 (1999).

[53] M. Glück, E. Reya, A. Vogt, Eur. Phys. J. **C5**, 461 (1998).

[54] A. De Rujula, S. L. Glashow, H. D. Politzer, S. B. Treiman, F. Wilczek and A. Zee, Phys. Rev. D **10**, 1649 (1974).

[55] E. Ruiz Arriola, Nucl. Phys. A **641**, 461 (1998).

[56] P. J. Sutton, A. D. Martin, R. G. Roberts, and W. J. Stirling, Phys. Rev. **D 45**, 2349 (1992).

[57] W. Broniowski and E. Ruiz Arriola, proc. of *Light cone physics: Hadrons and beyond*, IPPP, University of Durham, UK, 5-9 August 2003, ed. S. Dalley, p. 166, arXiv:hep-ph/0310048.

[58] J. S. Conway *et al.*, Phys. Rev. D **39**, 92 (1989).

[59] A. Peterman, Phys. Rept. **53**, 157 (1979).

[60] K. Golec-Biernat, *Deep inelastic scattering at small values of the Bjorken variable x*, habilitation thesis, INP Cracow report 1877/PH, August 2001, http://www.ifj.edu.pl/reports/1877.pdf.

[61] `http://www.mathworld.com`

[62] http://functions.wolfram.com/ HypergeometricFunctions/Hypergeometric1F2/06/02/04

[63] http://functions.wolfram.com/ HypergeometricFunctions/HypergeometricPFQ/06/04